Optimized Schwarz and Finite Element Cell-Centered Method for Heterogeneous Anisotropic Diffusion Problems

Thanh Hai Ong[a,1], Thi-Thao-Phuong Hoang[b,2,*]

[a] *Department of Analysis, Faculty of Mathematics & Computer Science, University of Science, VNU-HCMC, Ho Chi Minh City 700000, Vietnam.*
[b] *Department of Mathematics and Statistics, Auburn University, Auburn, AL 36849, USA.*

Abstract

The paper is concerned with the derivation and analysis of the optimized Schwarz type method for heterogeneous, anisotropic diffusion problems discretized by the finite element cell-centered (FECC) scheme. Differently from the standard finite element method (FEM), the FECC method involves only cell unknowns and satisfies local conservation of fluxes by using a technique of dual mesh and multipoint flux approximations to construct the discrete gradient operator. Consequently, if the domain is decomposed into nonoverlapping subdomains, the transmission conditions (on the interfaces between subdomains) associated with the FECC scheme are different from those of the standard FEM. We derive discrete Robin-type transmission conditions in the framework of FECC discretization, which include both weak and strong forms of the Robin terms due to the construction of the FECC's discrete gradient operator. Convergence of the associated iterative algorithm for a decomposition into strip-shaped subdomains is rigorously proved. Two dimensional numerical results for both isotropic and anisotropic diffusion tensors with large jumps in the coefficients are presented to illustrate the performance of the proposed methods with optimized Robin parameters.

Keywords: nonoverlapping domain decomposition, heterogeneous anisotropic coefficients, cell-centered schemes, finite elements, optimized Schwarz, discrete Robin transmission conditions

*Corresponding author.
Email addresses: `othai@hcmus.edu.vn` (Thanh Hai Ong), `tzh0059@auburn.edu` (Thi-Thao-Phuong Hoang)

[1] T.H. Ong's work is supported by the Vietnam National Foundation for Science and Technology Development (NAFOSTED) under grant number 107.02 − 2018.28. A part of the paper was completed during a scientific stay of the first author at the Vietnam Institute for Advanced Study in Mathematics (VIASM) whose hospitality is gratefully appreciated.

[2] T.-T.-P. Hoang's work is partially supported by the US National Science Foundation under grant number DMS-1912626 and Auburn University's intramural grants program.

1. Introduction

Heterogeneous anisotropic diffusion problems are important mathematical models used in various areas of science and engineering such as petroleum engineering, image processing or plasma physics. There exist two main difficulties in finding approximate solutions of these problems: firstly, for general problems with a heterogeneous and anisotropic (possibly with large discontinuities) tensor, it is hardly possible for numerical methods to obtain an approximate solution which converges to the weak solution of the problem; secondly, it is challenging to design numerical methods which can handle general two or three dimensional meshes. The finite element cell-centered (FECC) method is a numerical scheme which has been recently introduced and analyzed in [1, 2] for two- and three-dimensional diffusion problems. Unlike the standard FEM method which fails to give accurate approximations to problems with discontinuous coefficients, the FECC method can be applied to heterogeneous, anisotropic diffusion problems. Based on the construction of a dual mesh and a dual sub-mesh, and the use of multipoint flux approximations [3], the FECC scheme is cell-centered, satisfies local continuity of fluxes and can be applied on general (possibly distorted) meshes. Note that the finite volume element (FVE) method [4, 5, 6] also uses a dual mesh, but it is not a cell-centered scheme and only works on a triangular or quadrilateral primal mesh. In addition, in the FECC scheme the fluxes are enforced to be continuous across the primal edges while in the FVE method the fluxes are continuous across the dual edges. In [1], rigorous convergence analysis of the FECC method was carried out and numerical results indicate that on the same primal mesh, the FECC scheme gives more accurate solutions than those by the FEM [7], the finite volume method (FVM) [8, 9], the mixed finite volume method (MFV) [10], the mimetic finite difference method (MFD) [11], the compact-stencil MPFA method [12], the discrete duality finite volume method (DDFV) [13] and the SUSHI method [14]. An extension of the FECC scheme, namely the staggered cell-centered finite element method (SC-FEM), to two- and three-dimensional compressible and nearly-incompressible linear elasticity problems has been studied in [15, 16]. The SC-FEM is based on a mixed pressure-displacement formulation and is shown, by using the macroelement technique, to be stable and convergent with low-order (P0-P1) approximations for the pressure and the displacement.

For large-scale and heterogeneous problems, domain decomposition (DD) methods have become a powerful tool to perform parallel numerical simulations on multiprocessor supercomputers. There is a large amount of research and numerical algorithms using DD techniques for different types of linear and nonlinear partial differential equations (see [17, 18, 19] and the references therein). There are basically two types of DD methods with nonoverlapping subdomains: the formulation based on the Steklov-Poincaré operator [20, 21, 22], and Schwarz iterations with Robin transmission conditions [23] or with optimized transmission conditions [24, 25, 26, 27, 28]. The latter, known as the optimized Schwarz method, has attracted great attention of researchers during the last two decades as the use of general transmission conditions with optimized parameters significantly en-

hances the convergence rate of the associated iterative algorithms as well as efficiently handles the discontinuous coefficients [29, 30, 31, 32]. The idea of optimized transmission conditions has also been applied to improve the performance of Schwarz Waveform Relaxation methods for time-dependent problems with discontinuous coefficients, for instance in [33, 34, 35, 36, 37, 38].

The aim of this work is to develop and analyze the nonoverlapping optimized Schwarz methods for the FECC discretization of the diffusion problems with discontinuous, anistropic coefficients. Due to the specific construction of the FECC's discrete gradient operator, the transmission conditions associated with the FECC method are essentially different from those of the FEM. In particular, in addition to the continuity of the nodal unknowns and weak fluxes on the interfaces between subdomains, extra transmission conditions representing the continuity of fluxes in strong form are introduced. These conditions are required to obtain the equivalence between the discrete multidomain problem and the discrete monodomain problem. Furthermore, instead of using the physical transmission conditions on the interfaces, we derive equivalent Robin-type transmission conditions in the framework of the FECC scheme which include both weak and strong forms of the Robin terms. The new transmission conditions involve optimized parameters to enhance the information exchange between subdomains and handle the discontinuous coefficients. We reformulate the problems in the subdomains with discrete Robin-type transmission conditions as an *interface problem* which is solved iteratively by either Jacobi iteration or GMRES. The former leads to an iterative algorithm, namely the Robin-to-Robin algorithm, and we prove that it is convergent, for a decomposition into strips, as the number of iterations goes to infinity. Numerical experiments for two subdomains are carried out to investigate the performance of the proposed domain decomposition-based FECC method on heterogenenous, anisotropic diffusion problems. For multiple subdomains with cross points, the method can be generalized using auxiliary variables at the cross points [39, 40] together with a coarse problem to remove subdomain singularities as well as to enhance the scalability when the number of subdomains increases. However, this subject is beyond the scope of this paper and will be discussed elsewhere.

For an open, bounded domain Ω in $\mathbb{R}^d$ with Lipschitz boundary $\partial\Omega$, we consider the second order elliptic problem:

$$\begin{aligned} -\text{div } (\Lambda(\boldsymbol{x})\nabla u(\boldsymbol{x})) &= f(\boldsymbol{x}) \quad \text{in } \Omega, \\ u &= 0 \qquad \text{on } \partial\Omega, \end{aligned} \tag{1.1}$$

where $\Lambda : \Omega \to \mathbb{R}^{d\times d}$ is a symmetric, positive definite tensor such that Λ is piecewise Lipschitz-continuous on Ω and its eigenvalues are bounded in $\left[\underline{\lambda}, \overline{\lambda}\right]$, with $\underline{\lambda}, \overline{\lambda} > 0$. The function f is the source term and belongs to $L^2(\Omega)$. For simplicity, homogeneous Dirichlet boundary conditions are imposed. The analysis given below can be extended to other types of boundary conditions as in [17, Chapter 1, Section 1.4].

The weak form of problem (1.1) is given by:

$$\text{Find } u \in H_0^1(\Omega) \text{ such that}$$
$$\int_\Omega (\Lambda(\boldsymbol{x})\nabla u(\boldsymbol{x})) \cdot \nabla v(\boldsymbol{x})\, d\boldsymbol{x} = \int_\Omega f(\boldsymbol{x}) v(\boldsymbol{x})\, d\boldsymbol{x}, \quad \forall v \in H_0^1(\Omega). \tag{1.2}$$

It is well-known (see, for instance, [41, Chapter 1]) that under the assumptions made above, problem (1.2) has a unique solution $u \in H_0^1(\Omega)$.

In the next section, we introduce the FECC scheme for the discretization of problem (1.2). Then in Section 3, we derive the discrete multidomain problem using conforming decomposition, and formulate the discrete interface problem with Robin-type transmission conditions; from that we propose the Robin-to-Robin iterative algorithm and demonstrate its convergence. Finally, numerical results confirming theoretical analysis are presented in Section 4.

2. The FECC framework

In this section, we present the derivation of the FECC scheme [1] for problem (1.2) with heterogeneous, anisotropic coefficients: we first describe the construction of the meshes, then we define the discrete gradient which satisfies local conservation of fluxes; finally we derive a linear algebraic system associated with (1.2).

2.1. The meshes

For completeness, we recall the construction of the meshes in the FECC scheme as presented in [1, 2, 15]. In this work, we consider the two-dimensional case and derive the corresponding multidomain formulations (note that the FECC scheme has been studied for three-dimensional problems in [2, Chapter 3]).

For a polygonal domain $\Omega \subset \mathbb{R}^2$, we consider a general partition $\mathcal{T}_h$ of Ω:

$$\overline{\Omega} = \bigcup_{K \in \mathcal{T}_h} K.$$

We assume that each element $K \in \mathcal{T}_h$ is a star-shaped polygon in which we choose a point $C_K \in \text{int}(K)$ and call it the mesh point of K. Throughout the paper, we refer to $\mathcal{T}_h$ as the primal mesh. Next, we define the dual mesh $\mathcal{T}_h^*$ and the dual sub-mesh $\mathcal{T}_h^{**}$. For this purpose, we assume that the line joining two mesh points of any two neighboring elements is inside Ω and it intersects the common edge of the two elements. The latter assumption is necessary to define the scheme for heterogeneous problems (see [1]).

The dual mesh $\mathcal{T}_h^*$ is constructed from the primal mesh in such a way that each dual control volume of $\mathcal{T}_h^*$ corresponds to a vertex of $\mathcal{T}_h$. Denote by $\mathcal{N}$ the set of all nodes or vertices of $\mathcal{T}_h$:

$$\mathcal{N} := \{\mathfrak{I} : \mathfrak{I} \text{ is a vertex of element } K, \text{ for all } K \in \mathcal{T}_h\}.$$

For each $\mathfrak{I} \in \mathcal{N}$, denote by

$$\mathcal{K}_{\mathfrak{I}} := \{K \in \mathcal{T}_h : \text{ K shares the vertex } \mathfrak{I}\},$$

the set of primal elements that have $\mathfrak{I}$ as their vertex. We consider two cases (see Figure 1):

(a) If $\mathfrak{I}$ is an interior vertex, we obtain the dual control volume $M_{\mathfrak{I}}$ associated with the vertex $\mathfrak{I}$ by connecting the mesh points of neighboring elements in $\mathcal{K}_{\mathfrak{I}}$.

(b) If $\mathfrak{I}$ is on the boundary $\partial\Omega$ and assume that K_E and K_F are two (same or different) elements in $K_{\mathfrak{I}}$. Denote by $E \subset \partial K_E$ and $F \subset \partial K_F$ the two edges on the boundary that have $\mathfrak{I}$ as their vertex. The dual control volume $M_{\mathfrak{I}}$ is defined by joining mesh points of neighboring elements in $\mathcal{K}_{\mathfrak{I}}$ and the mesh point of K_E (and K_F) with a chosen interior point (e.g. the midpoint) of E (and F respectively). Note that in this case $M_{\mathfrak{I}}$ has $\mathfrak{I}$ as its vertex as well.

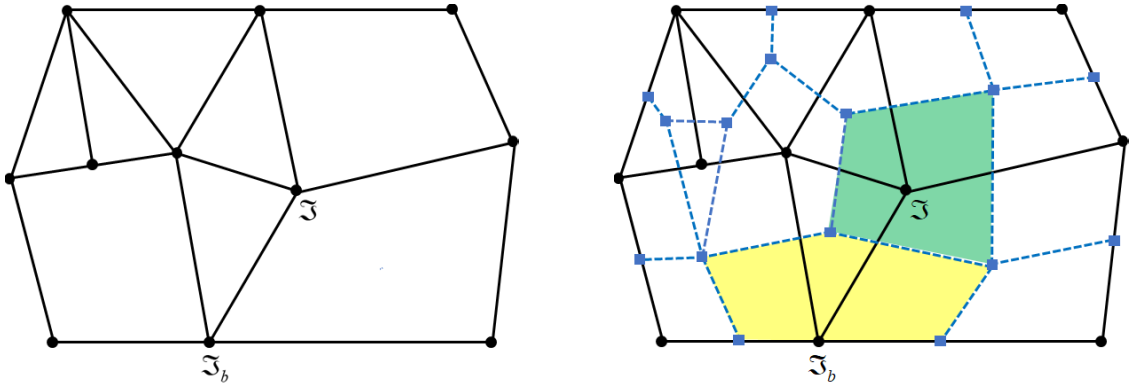

Figure 1: Left: The primal mesh $\mathcal{T}_h$ (solid lines) and its nodes (black); Right: The dual mesh $\mathcal{T}_h^*$ (blue dashed lines) and its nodes (blue). Examples of two dual control volumes (green and yellow polygons) corresponding to an internal node $\mathfrak{I}$ and a boundary node $\mathfrak{I}_b$ of the primal mesh $\mathcal{T}_h$, respectively.

The collection of all $M_{\mathfrak{I}}$ defines a dual mesh $\mathcal{T}_h^*$ such that

$$\overline{\Omega} = \bigcup_{\mathfrak{I} \in \mathcal{N}} M_{\mathfrak{I}}.$$

As for $\mathcal{T}_h$, we denote by $C_{M_{\mathfrak{I}}}$ the mesh point of $M_{\mathfrak{I}} \in \mathcal{T}_h^*$ which is chosen to be the corresponding vertex $\mathfrak{I}$ of the primal mesh:

$$C_{M_{\mathfrak{I}}} \equiv \mathfrak{I}, \quad \text{for all } M_{\mathfrak{I}} \in \mathcal{T}_h^*. \tag{2.1}$$

In what follows, we may drop the subscript $\mathfrak{I}$ to simplify the notation. We finally construct the dual sub-mesh $\mathcal{T}_h^{**}$ as a triangular subgrid of the dual grid as follows: for a dual control

volume $M \in \mathcal{T}_h^*$, we construct elements T of $\mathcal{T}_h^{**}$ by connecting the mesh point C_M to all vertices of M (see Figure 2):

$$\overline{\Omega} = \bigcup_{T \in \mathcal{T}_h^{**}} \overline{T}.$$

Let $\mathcal{N}^{**}$ be the set of nodes of elements of $\mathcal{T}_h^{**}$. We have the following remark.

Remark 2.1. *By construction, we have that:*

(a) for all interior triangular elements $T \in \mathcal{T}_h^{**}$ (i.e. $\partial T \cap \partial\Omega = \emptyset$), there exits two primal elements K and $L \in \mathcal{T}_h$ such that $T \cap K \neq \emptyset$ and $T \cap L \neq \emptyset$.

(b) $\mathcal{N}^{**}$ consists of three sets $\mathcal{C}$, $\mathcal{C}^*$ and $\mathcal{N}_{\partial\Omega}^{**}$ containing mesh points of primal elements, mesh points of dual control volumes and points lying on the boundary respectively:

$$\mathcal{N}^{**} = \mathcal{C} \cup \mathcal{C}^* \cup \mathcal{N}_{\partial\Omega}^{**}, \tag{2.2}$$

where $\mathcal{C} := \{C_K, \forall K \in \mathcal{T}_h\}$, $\mathcal{C}^* := \{C_M, \forall M \in \mathcal{T}_h^*\}$, and $\mathcal{N}_{\partial\Omega}^{**} := \{P \in \mathcal{N}^{**} \text{ such that } P \in \partial\Omega\}$.

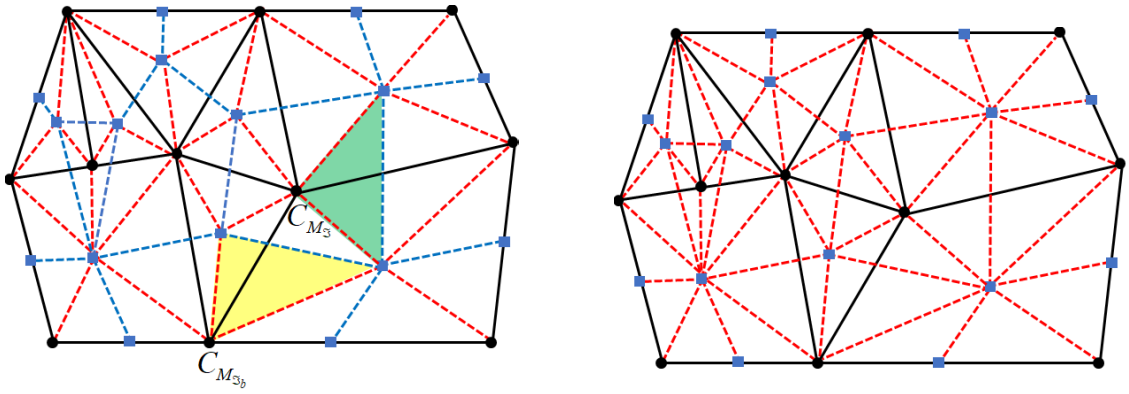

Figure 2: Left: Examples of two triangular elements (green and yellow triangles) of the dual sub-mesh created from the associated dual control volumes, note that the mesh point $C_{M_{\mathfrak{I}}}$ (respectively, $C_{M_{\mathfrak{I}_b}}$) is chosen to be the associated primal vertex $\mathfrak{I}$ (respectively, $\mathfrak{I}_b$) (see (2.1)); Right: The primal mesh $\mathcal{T}_h$ (black solid lines) and the dual sub-mesh $\mathcal{T}_h^{**}$ (red dashed lines).

On each primal element $K \in \mathcal{T}_h$, we denote the average of tensor Λ on K by:

$$\Lambda_K = \frac{1}{|K|} \int_K \Lambda(\boldsymbol{x}) d\boldsymbol{x}.$$

We aim to handle the heterogeneous, anisotropic case where Λ is discontinuous across the primal elements, i.e.:

$$\Lambda_K \neq \Lambda_L \qquad \text{for any } K, L \in \mathcal{T}_h,\ K \neq L. \tag{2.3}$$

The FECC scheme follows the idea of the standard finite element method applying on the dual sub-mesh and we seek for an approximate solution of problem (1.2) by finding its values at all nodes of the dual sub-mesh, $P \in \mathcal{N}^{**}$. Thus we define by X_h the set of all vectors $u_h := (u_P)_{P\in\mathcal{N}^{**}}$ where u_P is regarded as the approximate value of the solution u at the node $P \in \mathcal{N}^{**}$:

$$X_h = \left\{u_h = (u_P)_{P\in\mathcal{N}^{**}},\ u_P \in \mathbb{R}\right\}.$$

Due to Remark 2.1(b), we have that

$$u_h = (u_P)_{P\in\mathcal{N}^{**}} = \left((u_{C_K})_{K\in\mathcal{T}_h}, (u_{C_M})_{M\in\mathcal{T}_h^*}, (u_P)_{P\in\mathcal{N}_{\partial\Omega}^{**}}\right),$$

or simply, for the sake of exposition:

$$u_h = (u_P)_{P\in\mathcal{N}^{**}} = \left((u_K)_{K\in\mathcal{T}_h}, (u_M)_{M\in\mathcal{T}_h^*}, (u_P)_{P\in\mathcal{N}_{\partial\Omega}^{**}}\right), \tag{2.4}$$

with u_K and u_M the approximate values of u at the node C_K and C_M respectively. Recall that C_K is the mesh point of the primal element $K \in \mathcal{T}_h$ while C_M is the mesh point of the dual control volume $M \in \mathcal{T}_h^*$ which is chosen as in (2.1).

In addition, to handle Dirichlet boundary conditions, we need to define a subset of X_h, X_h^0, as follows:

$$X_h^0 = \{u_h \in X_h :\ u_P = 0, \quad \forall P \in \mathcal{N}_{\partial\Omega}^{**}\}.$$

In order to obtain the discrete variational formulation associated with problem (1.2), we shall define a projection operator $\Phi(u_h)$ and the discrete gradient $\nabla_\Lambda u_h$ for $u_h \in X_h$.

2.2. The projection operator and the discrete gradient

The two operators are defined by their restrictions to each triangular element T of $\mathcal{T}_h^{**}$. In particular, the projection operator $\Phi(u_h)$ is a function in $L^2(\Omega)$ and it is *continuous piecewise linear on each element* $T \in \mathcal{T}_h^{**}$, while the discrete gradient is defined in a way to enforce mass conservation in each element $T \in \mathcal{T}_h^{**}$ when the coefficient Λ is discontinuous (cf. (2.3) and Remark 2.1(a)).

We consider a triangle $T = (C_M C_K C_L) \in \mathcal{T}_h^{**}$ where K, L are two primal elements, $K, L \in \mathcal{T}_h$, and M a dual control volume, $M \in \mathcal{T}_h^*$ (see Figure 3). Denote by σ the common edge of K and L and $C_\sigma \in \sigma$ the intersecting point between the segment $C_K C_L$ and σ. For any $u_h \in X_h$, the restriction of $\Phi(u_h)$ to T, denoted by $\Phi_T(u_h)$, is a continuous function on T and it is linear on each of the two sub-triangles $(C_M C_\sigma C_K)$ and $(C_M C_\sigma C_L)$.

Let u_σ^M, *a temporary unknown* to be defined later, be an approximation of u_h at C_σ seeing from M.

In addition, denote by $\boldsymbol{n}_{C_M C_\sigma}^K$, $\boldsymbol{n}_{C_M C_K}$ and $\boldsymbol{n}_{C_K C_\sigma}$ the outward normal vectors of the triangle $(C_M C_\sigma C_K)$ such that the lengths of these vectors are equal to the segments $C_M C_\sigma$, $C_M C_K$ and $C_K C_\sigma$ respectively (see Figure 3). We also denote by $m_{(C_M C_\sigma C_K)}$ the measure of triangle $(C_M C_\sigma C_K)$. Remark that $\boldsymbol{n}_{C_M C_\sigma}^K + \boldsymbol{n}_{C_M C_\sigma}^L = 0$.

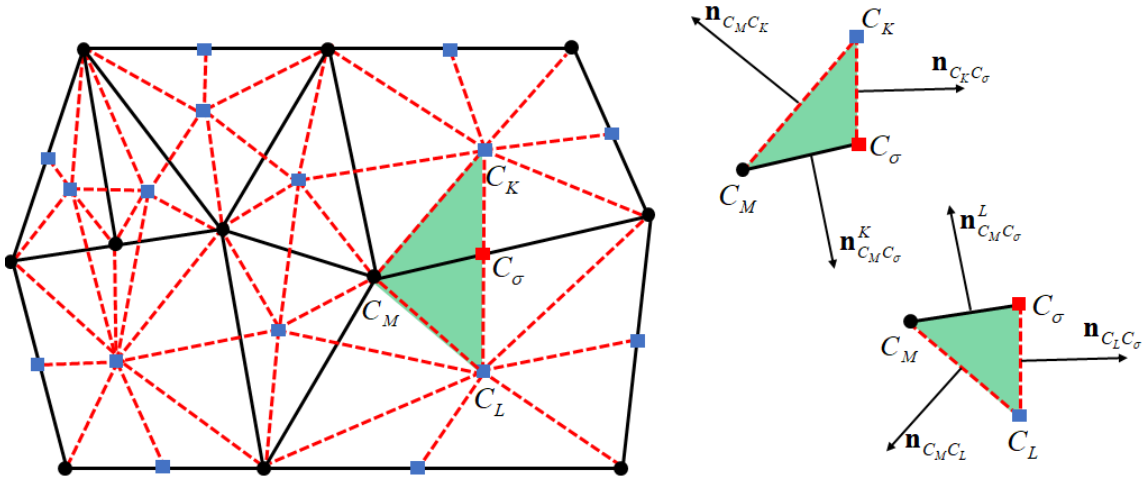

Figure 3: Left: An element (green) of the dual sub-grid $T = (C_M C_K C_L)$; Right: Outward normal vectors of the sub-triangle T.

For any vector $u_h \in X_h$, the projection operator $\Phi(u_h)$ and the discrete gradient $\nabla_\Lambda u_h$ restricted to T are defined as follows:

(i) On the triangle $(C_M C_\sigma C_K)$, we have

$$\Phi_T(u_h)|_{(C_M C_\sigma C_K)}(\boldsymbol{x}) = \begin{cases} u_M & \text{if } \boldsymbol{x} = \boldsymbol{x}_{C_M}, \\ u_K & \text{if } \boldsymbol{x} = \boldsymbol{x}_{C_K}, \\ u_\sigma^M & \text{if } \boldsymbol{x} = \boldsymbol{x}_{C_\sigma}. \end{cases}$$

Now using multi-point flux approximations, we define the restriction of $\nabla_\Lambda u_h$ on $(C_M C_\sigma C_K)$ as

$$\nabla_\Lambda u_h|_{(C_M C_\sigma C_K)} = \frac{-u_K \boldsymbol{n}^K_{C_M C_\sigma} - u_\sigma^M \boldsymbol{n}_{C_M C_K} - u_M \boldsymbol{n}_{C_K C_\sigma}}{2m_{(C_M C_\sigma C_K)}}. \tag{2.5}$$

Similarly, the restrictions of u_h and $\nabla_\Lambda u_h$ on triangle $(C_M C_\sigma C_L)$ are respectively

$$\Phi_T(u_h)|_{(C_M C_\sigma C_L)}(\boldsymbol{x}) = \begin{cases} u_M & \text{if } \boldsymbol{x} = \boldsymbol{x}_{C_M}, \\ u_L & \text{if } \boldsymbol{x} = \boldsymbol{x}_{C_L}, \\ u_\sigma^M & \text{if } \boldsymbol{x} = \boldsymbol{x}_{C_\sigma}, \end{cases}$$

and

$$\nabla_\Lambda u_h|_{(C_M C_\sigma C_L)} = \frac{-u_L \boldsymbol{n}^L_{C_M C_\sigma} - u_\sigma^M \boldsymbol{n}_{C_M C_L} - u_M \boldsymbol{n}_{C_L C_\sigma}}{2m_{(C_M C_\sigma C_L)}}. \tag{2.6}$$

(ii) Next, u_σ^M is determined to strongly satisfy the continuity of the flux across $C_M C_\sigma$:

$$\Lambda_K \nabla_\Lambda u_h|_{(C_M C_\sigma C_K)} \cdot \boldsymbol{n}^K_{C_M C_\sigma} + \Lambda_L \nabla_\Lambda u_h|_{(C_M C_\sigma C_L)} \cdot \boldsymbol{n}^L_{C_M C_\sigma} = 0. \tag{2.7}$$

Assume that

$$\Delta := \beta_{1,\sigma}^{M} + \beta_{2,\sigma}^{M} = -\frac{\left(\boldsymbol{n}_{C_M C_\sigma}^{K}\right)^t \Lambda_K \boldsymbol{n}_{C_M C_K}}{2m_{(C_M C_\sigma C_K)}} - \frac{\left(\boldsymbol{n}_{C_M C_\sigma}^{L}\right)^t \Lambda_L \boldsymbol{n}_{C_M C_L}}{2m_{(C_M C_\sigma C_L)}} \neq 0, \tag{2.8}$$

where $\boldsymbol{n}^t$ is the transpose of vector $\boldsymbol{n}$, then after performing some calculations on Equation (2.7) we deduce that

$$u_\sigma^M = \beta_M u_M + \beta_K u_K + \beta_L u_L, \tag{2.9}$$

where

$$\beta_K = \frac{1}{\Delta} \cdot \frac{\left(\boldsymbol{n}_{C_M C_\sigma}^{K}\right)^t \Lambda_K \boldsymbol{n}_{C_M C_\sigma}^{K}}{2m_{(C_M C_\sigma C_K)}}, \quad \beta_L = \frac{1}{\Delta} \cdot \frac{\left(\boldsymbol{n}_{C_M C_\sigma}^{L}\right)^t \Lambda_L \boldsymbol{n}_{C_M C_\sigma}^{L}}{2m_{(C_M C_\sigma C_L)}},$$
$$\beta_M = 1 - \beta_K - \beta_L.$$

Remark 2.2. *For each internal edge $\sigma \equiv C_M C_{\widehat{M}}$ of the primal elements, there are two values of u at C_σ, one seeing from M, u_σ^M and another from $\widehat{M}$, $u_\sigma^{\widehat{M}}$. As for u_σ^M, we have that $u_\sigma^{\widehat{M}}$ can be expressed as a linear combination of $u_{\widehat{M}}$, u_K and u_L. The triangles (C_M, C_K, C_L) and $(C_{\widehat{M}}, C_K, C_L)$ are distinct, thus the two values of u at C_σ are different: $u_\sigma^M \neq u_\sigma^{\widehat{M}}$. Note that for homogeneous Dirichlet boundary conditions, $u_\sigma^M = 0$ if $C_\sigma \in \partial\Omega$.*

Substituting (2.9) into (2.5) and (2.6), we conclude that the discrete gradient $\nabla_\Lambda u_h$ restricted to the triangle $T = (C_M C_K C_L) \in \mathcal{T}_h^{**}$ linearly depends on the three nodal values u_M, u_K and u_L:

$$\nabla_\Lambda u_h|_{(C_M C_\sigma C_K)} = \frac{-u_K \widetilde{\boldsymbol{n}}_{(C_M, C_\sigma, C_K)}^{K} - u_L \widetilde{\boldsymbol{n}}_{(C_M, C_\sigma, C_K)}^{L} - u_M \widetilde{\boldsymbol{n}}_{(C_M, C_\sigma, C_K)}^{M}}{2m_{(C_M C_\sigma C_K)}}, \tag{2.10}$$

$$\nabla_\Lambda u_h|_{(C_M C_\sigma C_L)} = \frac{-u_K \widetilde{\boldsymbol{n}}_{(C_M, C_\sigma, C_L)}^{K} - u_L \widetilde{\boldsymbol{n}}_{(C_M, C_\sigma, C_L)}^{L} - u_M \widetilde{\boldsymbol{n}}_{(C_M, C_\sigma, C_L)}^{M}}{2m_{(C_M C_\sigma C_L)}}, \tag{2.11}$$

with

$$\widetilde{\boldsymbol{n}}_{(C_M, C_\sigma, C_K)}^{K} = \boldsymbol{n}_{C_M C_\sigma}^{K} + \beta_K \boldsymbol{n}_{C_M C_K}, \quad \widetilde{\boldsymbol{n}}_{(C_M, C_\sigma, C_K)}^{L} = \beta_L \boldsymbol{n}_{C_M C_K},$$
$$\widetilde{\boldsymbol{n}}_{(C_M, C_\sigma, C_K)}^{M} = \boldsymbol{n}_{C_K C_\sigma} + \beta_M \boldsymbol{n}_{C_M C_K}, \quad \widetilde{\boldsymbol{n}}_{(C_M, C_\sigma, C_L)}^{K} = \beta_K \boldsymbol{n}_{C_M C_L},$$
$$\widetilde{\boldsymbol{n}}_{(C_M, C_\sigma, C_L)}^{L} = \boldsymbol{n}_{C_M C_\sigma}^{L} + \beta_L \boldsymbol{n}_{C_M C_L}, \quad \widetilde{\boldsymbol{n}}_{(C_M, C_\sigma, C_L)}^{M} = \boldsymbol{n}_{C_L C_\sigma} + \beta_M \boldsymbol{n}_{C_M C_L}.$$

With the above defined operators, we obtain the discrete variational formulation associated with problem (1.2) as follows:

Find $u_h \in X_h^0$ such that

$$\int_\Omega (\Lambda(\boldsymbol{x}) \nabla_\Lambda u_h(\boldsymbol{x})) \cdot \nabla_\Lambda v_h(\boldsymbol{x})\, d\boldsymbol{x} = \int_\Omega f(\boldsymbol{x}) \Phi(v_h)(\boldsymbol{x})\, d\boldsymbol{x}, \ \forall v_h \in X_h^0. \tag{2.12}$$

2.3. The linear algebraic system

To derive the linear algebraic system associated with (2.12), for each $Q \in (\mathcal{N}^{**} \setminus \mathcal{N}^{**}_{\partial\Omega})$ (Q does not lie on the boundary), we choose $v_h = v_h^Q = \left(v_P^Q\right)_{P\in\mathcal{N}^{**}} \in X_h^0$ such that

$$v_P^Q = \begin{cases} 1 & \text{if } P \equiv Q, \\ 0 & \text{if } P \neq Q, \end{cases} \tag{2.13}$$

and obtain

$$\int_\Omega (\Lambda(\boldsymbol{x})\nabla_\Lambda u_h(\boldsymbol{x})) \cdot \nabla_\Lambda v_h^Q(\boldsymbol{x})\, d\boldsymbol{x} = \int_\Omega f(\boldsymbol{x})\Phi(v_h^Q)(\boldsymbol{x})\, d\boldsymbol{x}, \quad \forall Q \in (\mathcal{N}^{**} \setminus \mathcal{N}^{**}_{\partial\Omega}), \tag{2.14}$$

in which the discrete gradient depends only on the nodal values u_P, $P \in \mathcal{N}^{**}$ (cf. formulas (2.10) and (2.11)).

To derive a matrix form of (2.14), notice that the set $(\mathcal{N}^{**} \setminus \mathcal{N}^{**}_{\partial\Omega})$ consists of all mesh points C_K of the primal elements and all mesh points C_M of the dual control volumes (see Remark 2.1(b)). Thus we proceed as in [1, pp. 12-14] by first choosing $v_h = v_h^{C_M}$ for each $M \in \mathcal{T}_h^*$ in (2.14) and obtain the linear system:

$$\boldsymbol{D}u_h|_{\mathcal{T}_h^*} + \boldsymbol{E}u_h|_{\mathcal{T}_h} = \boldsymbol{F}^*, \tag{2.15}$$

where $u_h|_{\mathcal{T}_h^*} := (u_M)_{M\in\mathcal{T}_h^*}$ and $u_h|_{\mathcal{T}_h} := (u_K)_{K\in\mathcal{T}_h}$, $\boldsymbol{D}$ is a diagonal matrix with positive entries (see [1]) and $\boldsymbol{F}^*$ a column matrix depending on f. Next, we take $v_h = v_h^{C_K}$ for each $K \in \mathcal{T}_h$:

$$\boldsymbol{M}u_h|_{\mathcal{T}_h^*} + \boldsymbol{N}u_h|_{\mathcal{T}_h} = \boldsymbol{F}, \tag{2.16}$$

where $\boldsymbol{N}$ is a symmetric, square matrix, $\boldsymbol{F}$ a column matrix depending on f and $\boldsymbol{M}$ is the transpose matrix of $\boldsymbol{E}$.

Hence, the matrix system associated with (2.14) is

$$\begin{pmatrix} \boldsymbol{D} & \boldsymbol{E} \\ \boldsymbol{M} & \boldsymbol{N} \end{pmatrix} \begin{pmatrix} u_h|_{\mathcal{T}_h^*} \\ u_h|_{\mathcal{T}_h} \end{pmatrix} = \begin{pmatrix} \boldsymbol{F}^* \\ \boldsymbol{F} \end{pmatrix}. \tag{2.17}$$

Since $\boldsymbol{D}$ is diagonal, one can compute $\boldsymbol{U}^*$ from the first equation of (2.17):

$$u_h|_{\mathcal{T}_h^*} = \boldsymbol{D}^{-1}(\boldsymbol{F}^* - \boldsymbol{E}u_h|_{\mathcal{T}_h}).$$

Substituting this into the second equation of (2.17), we obtain the following linear system involving only primal cell unknowns $(u_K)_{K\in\mathcal{T}_h}$:

$$\left(\boldsymbol{N} - \boldsymbol{M}\boldsymbol{D}^{-1}\boldsymbol{E}\right) u_h|_{\mathcal{T}_h} = \boldsymbol{F} - \boldsymbol{M}\boldsymbol{D}^{-1}\boldsymbol{F}^*,$$

The matrix $\boldsymbol{A} := \boldsymbol{N} - \boldsymbol{M}\boldsymbol{D}^{-1}\boldsymbol{E}$ is a variant of the stiffness matrix. Under assumption (2.8), $\boldsymbol{A}$ is symmetric and positive definite on general meshes [1].

We also recall Corollary 5.4 in [1] that the FECC scheme is convergent, that is to say, $\Phi(u_h)$ converges to the exact solution u_{exact} the problem and $\nabla_\Lambda u_h$ tends to ∇u_{exact} as $h \to 0$, with $h = \sup\{h_T,$ the diameter of the triangle T, $T \in \mathcal{T}_h^{**}\}$.

3. Nonoverlapping, optimized Schwarz algorithm

We present the derivation and convergence analysis of the optimized Schwarz algorithm based on the FECC discretization and nonoverlapping subdomains. In Subsection 3.1, we first introduce the setting for domain decomposition, and construct the discrete physical transmission conditions associated with the FECC scheme. Then, in Subsection 3.2, more general transmission conditions of Robin-type are derived and an associated interface problem is introduced. Finally in Subsection 3.3, we present the Robin-to-Robin iterative algorithm resulting from solving the interface problem by Jacobi iteration and prove its convergence for strip-shaped subdomains.

3.1. Conforming domain decomposition and discrete transmission conditions

We consider a partition $\mathcal{T}_h$ of Ω and a conforming decomposition of Ω into nonoverlapping subdomains. For simplicity of presentation, we consider the case of two subdomains Ω_1 and Ω_2. The analysis can be extended to many subdomain case with strip substructures (see Subsection 3.3). Denote by Γ the interface between the two subdomains: $\Gamma = \partial\Omega_1 \cap \partial\Omega_2 \cap \Omega$.

Let $\mathcal{T}_{h,i}$, $i = 1, 2$, be the partition of Ω_i such that $\mathcal{T}_{h,i}$ is a subset of $\mathcal{T}_h$. We shall construct the dual mesh $\mathcal{T}_{h,i}^*$ and the dual sub-mesh $\mathcal{T}_{h,i}^{**}$ of the subdomains from those of the monodomain, $\mathcal{T}_h^*$ and $\mathcal{T}_h^{**}$. Since each dual control volume corresponds to a vertex of the primal mesh, we distinguish two cases (see Figure 4):

(a) If the vertex $\mathfrak{I}$ of an element of $\mathcal{T}_{h,i}$ does not belong to Γ, then its control volume $M_{\mathfrak{I}}^i \in \mathcal{T}_{h,i}^*$ coincides with the control volume $M_{\mathfrak{I}}$ of $\mathcal{T}_h^*$. Hence, the triangular elements of $\mathcal{T}_{h,i}^{**}$ associated with $M_{\mathfrak{I}}^i$ are those of $\mathcal{T}_h^{**}$ associated with $M_{\mathfrak{I}}$.

(b) Otherwise if $\mathfrak{I} \in \Gamma$ (note that Γ now is a part of the boundary of Ω_i), its control volume $M_{\mathfrak{I}}^i \in \mathcal{T}_{h,i}^*$ is the intersection of the control volume $M_{\mathfrak{I}} \in \mathcal{T}_h^*$ and $\overline{\Omega_i}$. The triangular elements of $\mathcal{T}_{h,i}^{**}$ associated with $M_{\mathfrak{I}}^i$ is then defined as in Subsection 2.1.

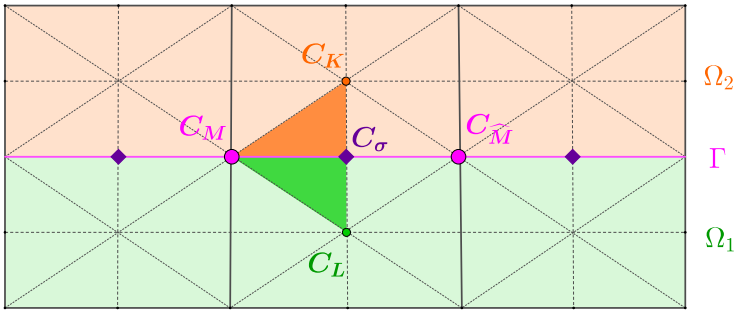

Figure 4: Conforming discretizations in the subdomains.

The dual sub-meshes $\mathcal{T}_{h,1}^{**}$ and $\mathcal{T}_{h,2}^{**}$ are matching on the interface Γ and they are not subsets of $\mathcal{T}_h^{**}$. Denote by $\mathcal{N}_i^{**}$, $i = 1, 2$, the set of all vertices of elements of $\mathcal{T}_{h,i}^{**}$. Note

that $\mathcal{N}_1^{**}$ and $\mathcal{N}_2^{**}$ are not subsets of $\mathcal{N}^{**}$ (recall that $\mathcal{N}^{**}$ is the set of all vertices of $\mathcal{T}_h^{**}$). As for the monodomain case (cf. Remark 2.1(b) and (2.2)), we can decompose $\mathcal{N}_{h,i}^{**}$ into three sets $\mathcal{C}_i$, $\mathcal{C}_i^*$ and $\mathcal{N}_{i,\partial\Omega_i}^{**}$ as follows:

$$\mathcal{N}_i^{**} = \mathcal{C}_i \ \cup \ \mathcal{C}_i^* \ \cup \ \mathcal{N}_{i,\partial\Omega_i}^{**}, \tag{3.1}$$

where $\mathcal{C}_i := \{C_K, \ \forall K \in \mathcal{T}_{h,i}\}$, $\mathcal{C}_i^* := \left\{C_M, \ \forall M \in \mathcal{T}_{h,i}^*\right\}$,
and $\mathcal{N}_{i,\partial\Omega_i}^{**} := \{P \in \mathcal{N}_i^{**} \text{ such that } P \in \partial\Omega_i\}$.

We denote by $\mathcal{N}_\Gamma^{**}$ the set of vertices of elements of $\mathcal{T}_{h,i}^{**}$, $i = 1, 2$, that belong to Γ and by $\mathcal{E}_\Gamma^{**}$ the set of edges of elements of $\mathcal{T}_{h,i}^{**}$ that lie on Γ. Let $\mathcal{N}_{\Gamma,\circ}^{**}$ be a subset of $\mathcal{N}_\Gamma^{**}$ consisting of the nodes of the primal mesh $\mathcal{T}_{h,i}$ lying on Γ (magenta circled points in Figure 4), and define $\mathcal{N}_{\Gamma,\square}^{**} := \mathcal{N}_\Gamma^{**} \setminus \mathcal{N}_{\Gamma,\circ}^{**}$. The points in $\mathcal{N}_{\Gamma,\square}^{**}$ (purple squared points in Figure 4) result from case (b) above and they play the same role as C_σ in the construction of the discrete gradient (Subsection 2.2). Note that $\mathcal{N}_{\Gamma,\square}^{**} \cap \mathcal{N}^{**} = \emptyset$.

To derive the formulation for the subdomain problems, we introduce the sets:

$$\begin{aligned} X_{h,i} &:= \left\{u_{h,i} = (u_{i,P})_{P\in\mathcal{N}_i^{**}}, \ u_{i,P} \in \mathbb{R}\right\}, \\ X_{h,i}^{0,\partial\Omega_i\cap\partial\Omega} &:= \left\{u_{h,i} \in X_{h,i} : \ u_{i,P} = 0, \ \forall P \in \left(\mathcal{N}_{i,\partial\Omega_i}^{**} \setminus \mathcal{N}_\Gamma^{**}\right)\right\}, \end{aligned}$$

for $i = 1, 2$, and the space

$$\mathcal{G}_h := \left\{\Phi(v_h)|_\Gamma, \forall v_h \in X_h^0\right\} \subset L^2(\Gamma). \tag{3.2}$$

By the construction of the discrete gradient (cf. Subsection 2.2), we have that functions in $\mathcal{G}_h$ are discontinuous on Γ and piecewise linear on the interface edges $e \in \mathcal{E}_\Gamma^{**}$. We also define the set of vectors $u_{h,\Gamma}$ containing the nodal unknowns on the interface: $G_h := \left\{u_{h,\Gamma} = (u_P)_{P\in\mathcal{N}_\Gamma^{**}}, \ u_P \in \mathbb{R}\right\}$. Finally, we define the projection Φ_i, the discrete gradient $\nabla_{\Lambda,i}$ and the right-hand side data f_i for $i = 1, 2$, as the restrictions of Φ, ∇_Λ and f to Ω_i respectively.

With such notation, the discrete multidomain problem equivalent to the monodomain problem (2.14) consists of:

1. solving in the subdomains the following problems:

   Find $u_{h,i} \in X_{h,i}^{0,\partial\Omega_i\cap\partial\Omega}$ such that

   $$\int_{\Omega_i} (\Lambda_i \nabla_{\Lambda,i} u_{h,i}) \cdot \nabla_{\Lambda,i} v_{h,i} \, d\boldsymbol{x} - \int_\Gamma (\Lambda_i \nabla_{\Lambda,i} u_{h,i}) \cdot \boldsymbol{n}_i \Phi_i(v_{h,i}) d\gamma = \int_{\Omega_i} f_i \Phi_i(v_{h,i}) \, d\boldsymbol{x},$$
   $$\forall v_{h,i} \in X_{h,i}^{0,\partial\Omega_i\cap\partial\Omega}, \text{ for } i = 1, 2, \tag{3.3}$$

2. together with three transmission conditions on Γ expressing respectively:

(a) the continuity of the solution on Γ:

$$\Phi_1(u_{h,1})|_\Gamma = \Phi_2(u_{h,2})|_\Gamma, \tag{3.4}$$

or equivalently, with $M,\ \widehat{M} \in \mathcal{T}_h^*$ such that $C_\sigma \in C_M C_{\widehat{M}}$,

$$u_{1,\sigma}^M = u_{2,\sigma}^M, \quad u_{1,\sigma}^{\widehat{M}} = u_{2,\sigma}^{\widehat{M}}, \quad \forall C_\sigma \in \mathcal{N}_{\Gamma,\square}^{**}, \tag{3.5}$$

$$u_{1,P} = u_{2,P}, \quad \forall P \in \mathcal{N}_{\Gamma,\circ}^{**}, \tag{3.6}$$

(b) the continuity (in strong form) of the flux in each element of $\mathcal{T}_h^{**}$ that intersects the interface Γ:

$$\int_e \sum_{i=1}^{2} (\Lambda_i \nabla_{\Lambda,i} u_{h,i} \cdot \boldsymbol{n}_i)\, d\gamma = 0, \quad \forall e \in \mathcal{E}_\Gamma^{**}, \tag{3.7}$$

(c) and the continuity of the flux across Γ:

$$\int_\Gamma \left(\sum_{i=1}^{2} \Lambda_i \nabla_{\Lambda,i} u_{h,i} \cdot \boldsymbol{n}_i \right) \gamma_h \, d\gamma = 0, \quad \forall \gamma_h \in \mathcal{G}_h. \tag{3.8}$$

The first and third transmission conditions (cf. (3.4) and (3.8) respectively) are standard, while the second transmission condition (3.7) results from the construction of the discrete gradient in the FECC scheme and it is used to determine the values of the solution at points $C_\sigma \in \mathcal{N}_{\Gamma,\square}^{**}$.

We now examine in more detail the third transmission condition (3.8) in the context of the FECC scheme. We first determine vectors $v_h \in X_h^0$ such that $\Phi(v_h)|_\Gamma \neq 0$. One can easily see that

$$\Phi\left(v_h^Q\right)|_\Gamma \neq 0, \quad \forall Q \in \mathcal{N}_{\Gamma,\circ}^{**} \subset \mathcal{N}^{**}.$$

Recall that the test vector $v_h^Q \in X_h^0$ is defined as in (2.13). Furthermore, because of the construction of the discrete gradient, we also have

$$\Phi\left(v_h^Q\right)|_\Gamma \neq 0, \quad \forall Q \in \mathcal{C}_i^\Gamma,\ i = 1, 2, \tag{3.9}$$

where $\mathcal{C}_i^\Gamma$ is the set of mesh points of primal elements of Ω_i that have edges lying on Γ:

$$\mathcal{C}_i^\Gamma := \{C_K,\ K \in \mathcal{T}_{h,i},\ \partial K \cap \Gamma \neq \emptyset\},\ i = 1, 2.$$

In other words, the space $\mathcal{G}_h$ (3.2) consists of linear combinations of functions $\Phi\left(v_h^Q\right)|_\Gamma$, for all $Q \in \mathcal{N}_{\Gamma,\circ}^{**} \cup \mathcal{C}_1^\Gamma \cup \mathcal{C}_2^\Gamma$. As a consequence, the condition of flux continuity (3.8) can be replaced equivalently by

$$\int_\Gamma \left(\sum_{i=1}^{2} \Lambda_i \nabla_{\Lambda,i} u_{h,i} \cdot \boldsymbol{n}_i \right) \Phi\left(v_h^Q\right)\, d\gamma = 0, \quad \forall Q \in \mathcal{N}_{\Gamma,\circ}^{**}, \tag{3.10}$$

$$\int_\Gamma (\Lambda_1 \nabla_{\Lambda,1} u_{h,1} \cdot \boldsymbol{n}_1)\, \Phi\left(v_h^{Q_1}\right)\, d\gamma = \int_\Gamma (\Lambda_2 \nabla_{\Lambda,2} u_{h,2} \cdot \boldsymbol{n}_1)\, \Phi\left(v_h^{Q_1}\right)\, d\gamma, \quad \forall Q_1 \in \mathcal{C}_1^\Gamma, \tag{3.11}$$

$$\int_\Gamma (\Lambda_2 \nabla_{\Lambda,2} u_{h,2} \cdot \boldsymbol{n}_2)\, \Phi\left(v_h^{Q_2}\right)\, d\gamma = \int_\Gamma (\Lambda_1 \nabla_{\Lambda,1} u_{h,1} \cdot \boldsymbol{n}_2)\, \Phi\left(v_h^{Q_2}\right)\, d\gamma, \quad \forall Q_2 \in \mathcal{C}_2^\Gamma. \tag{3.12}$$

Note that the projection Φ is global (i.e. defined on the whole domain Ω). Next, we will transform these equations into a form that involves only local projections Φ_i, $i = 1, 2$.

For $Q \in \mathcal{N}^{**}_{\Gamma,\circ} \subset \Gamma$ (in Equation (3.10)): by definition of the projection Φ, it is clear that

$$\Phi\left(v_h^Q\right)|_\Gamma = \Phi_1\left(v_{h,1}^Q\right)|_\Gamma = \Phi_2\left(v_{h,2}^Q\right)|_\Gamma, \tag{3.13}$$

where $v_{h,i}^Q = \left(v_{i,P}^Q\right)_{P\in\mathcal{N}_i^{**}} \in X_{h,i}^{0,\partial\Omega_i\cap\partial\Omega}$, for $Q \in \mathcal{N}_i^{**}$ and $i = 1, 2$, is defined by

$$v_{i,P}^Q = \begin{cases} 1 & \text{if } P \equiv Q, \\ 0 & \text{if } P \neq Q,\ P \notin \mathcal{N}^{**}_{\Gamma,\square}. \end{cases} \tag{3.14}$$

For $Q_i \in \mathcal{C}_i^\Gamma \subset \Omega_i$ (in Equations (3.11) and (3.12)) with $i \in 1, 2$ fixed and $j = (3 - i)$: we have that

$$\Phi\left(v_h^{Q_i}\right)|_\Gamma = \Phi_i\left(v_{h,i}^{Q_i}\right)|_\Gamma .$$

Since $Q_i \in \Omega_i$, there does not exist a vector $v_{h,j}^{Q_i} \in X_{h,j}^{0,\partial\Omega_j\cap\partial\Omega}$. Consequently, we can not proceed as in the former case for Φ_j. Instead, we define $E_{h,j}$ as an extension operator from G_h to $X_{h,j}^{0,\partial\Omega_j\cap\partial\Omega}$ as follows: for $v_\Gamma = (v_P)_{P\in\mathcal{N}_\Gamma^{**}} \in G_h$, we have

$$E_{h,j}\left(v_\Gamma\right) = v_{h,j} := \begin{cases} v_P & \text{if } P \in \mathcal{N}_\Gamma^{**}, \\ 0 & \text{if } P \in \left(\mathcal{N}_j^{**} \setminus \mathcal{N}_\Gamma^{**}\right). \end{cases} \tag{3.15}$$

Then

$$\Phi\left(v_h^{Q_i}\right)|_\Gamma = \Phi_i\left(v_{h,i}^{Q_i}\right)|_\Gamma = \Phi_j\left(E_{h,j}(v_{i,\Gamma}^{Q_i})\right)|_\Gamma, \tag{3.16}$$

where $v_{i,\Gamma}^{Q_i} := \left(v_{i,P}^{Q_i}\right)_{P\in\mathcal{N}_\Gamma^{**}} \in G_h$.

Using the relations established in (3.13) and (3.16) we can rewrite the transmission conditions (3.10)-(3.12) as follows:

$$\int_\Gamma \sum_{i=1}^{2} \left(\Lambda_i \nabla_{\Lambda,i} u_{h,i} \cdot \boldsymbol{n}_i\right) \Phi_i\left(v_{h,i}^Q\right)\, d\gamma = 0, \quad \forall Q \in \mathcal{N}^{**}_{\Gamma,\circ}, \tag{3.17}$$

$$\int_\Gamma \left(\Lambda_1 \nabla_{\Lambda,1} u_{h,1} \cdot \boldsymbol{n}_1\right) \Phi_1\left(v_{h,1}^{Q_1}\right)\, d\gamma = \int_\Gamma \left(\Lambda_2 \nabla_{\Lambda,2} u_{h,2} \cdot \boldsymbol{n}_1\right) \Phi_2\left(E_{h,2}(v_{1,\Gamma}^{Q_1})\right)\, d\gamma, \quad \forall Q_1 \in \mathcal{C}_1^\Gamma, \tag{3.18}$$

$$\int_\Gamma \left(\Lambda_2 \nabla_{\Lambda,2} u_{h,2} \cdot \boldsymbol{n}_2\right) \Phi_2\left(v_{h,2}^{Q_2}\right)\, d\gamma = \int_\Gamma \left(\Lambda_1 \nabla_{\Lambda,1} u_{h,1} \cdot \boldsymbol{n}_2\right) \Phi_1\left(E_{h,1}(v_{2,\Gamma}^{Q_2})\right)\, d\gamma, \quad \forall Q_2 \in \mathcal{C}_2^\Gamma. \tag{3.19}$$

The last two equations are introduced due to the properties of the discrete gradient of the FECC scheme. Such equations are not present in the domain decomposition formulation with finite element discretizations (see [17, Chapter 2]).

3.2. Equivalent Robin-type transmission conditions and interface problem

With the aim of using more general transmission conditions to accelerate the convergence speed of the associated iterative algorithm, we extend the optimized Schwarz method with Robin transmission conditions to the FECC scheme. We first rewrite the transmission conditions (3.5)-(3.8) as follows:

$$\int\limits_{e=C_M C_\sigma} u_{1,\sigma}^{M}\, d\gamma = \int_e u_{2,\sigma}^{M}\, d\gamma, \quad \int\limits_{e=C_{\widehat{M}} C_\sigma} u_{1,\sigma}^{\widehat{M}}\, d\gamma = \int_e u_{2,\sigma}^{\widehat{M}}\, d\gamma, \quad \forall C_\sigma \in \mathcal{N}_{\Gamma,\square}^{**}, \tag{3.20}$$

where $M,\ \widehat{M} \in \mathcal{T}_{h,i}^{*}$ such that $C_\sigma \in C_M C_{\widehat{M}}$,

$$\int_e \Lambda_1 \nabla_{\Lambda,1} u_{h,1} \cdot \boldsymbol{n}_1\, d\gamma = -\int_e \Lambda_2 \nabla_{\Lambda,2} u_{h,2} \cdot \boldsymbol{n}_2\, d\gamma, \quad \forall e \in \mathcal{E}_\Gamma^{**}, \tag{3.21}$$

$$\begin{aligned}\int_\Gamma \left[\Lambda_1 \nabla_{\Lambda,1} u_{h,1} \cdot \boldsymbol{n}_1 + \alpha_{12}\Phi_1(u_{h,1})\right] \gamma_h d\gamma \\ = \int_\Gamma \left[\Lambda_2 \nabla_{\Lambda,2} u_{h,2} \cdot \boldsymbol{n}_1 + \alpha_{12}\Phi_2(u_{h,2})\right] \gamma_h d\gamma, \quad \forall \gamma_h \in \mathcal{G}_h,\end{aligned} \tag{3.22}$$

$$\begin{aligned}\int_\Gamma \left[\Lambda_2 \nabla_{\Lambda,2} u_{h,2} \cdot \boldsymbol{n}_2 + \alpha_{21}\Phi_2(u_{h,2})\right] \gamma_h d\gamma \\ = \int_\Gamma \left[\Lambda_1 \nabla_{\Lambda,1} u_{h,1} \cdot \boldsymbol{n}_2 + \alpha_{21}\Phi_1(u_{h,1})\right] \gamma_h d\gamma, \quad \forall \gamma_h \in \mathcal{G}_h,\end{aligned} \tag{3.23}$$

in which α_{12} and α_{21} are two positive parameters which are chosen to accelerate the convergence of the associated iterative algorithm. For precise details of how the optimization is carried out, see [26, 42]. Obviously, (3.20)-(3.23) can be deduced from (3.5)-(3.8). To prove the opposite, we subtract (3.23) from (3.22) and obtain:

$$(\alpha_{12} + \alpha_{21}) \int_\Gamma \left[\Phi_1(u_{h,1}) - \Phi_2(u_{h,2})\right] \gamma_h = 0, \quad \forall \gamma_h \in \mathcal{G}_h. \tag{3.24}$$

Since α_{12} and α_{21} are positive, (3.24) is equivalent to

$$\int_\Gamma \left(\Phi_1(u_{h,1}) - \Phi_2(u_{h,2})\right) \gamma_h = 0, \quad \forall \gamma_h \in \mathcal{G}_h. \tag{3.25}$$

By definition, the restrictions of $\Phi_1(u_{h,1})$, $\Phi_2(u_{h,2})$ to Γ and γ_h are piecewise linear on Γ. We choose $\gamma_h = \Phi(v_h^Q)$ with $Q \in \mathcal{N}_{\Gamma,\circ}^{**}$ and use the trapezoidal quadrature rule to deduce from (3.25) and (3.20) that

$$u_{1,Q} = u_{2,Q}, \quad \forall Q \in \mathcal{N}_{\Gamma,\circ}^{**}.$$

Consequently,

$$\Phi_1(u_{h,1}) = \Phi_2(u_{h,2}) \quad \text{on } \Gamma. \tag{3.26}$$

Substituting this into either (3.22) or (3.23), we obtain continuity of flux across Γ (in the weak sense).

Next we rewrite the equation (3.22) using local projections as in (3.17)-(3.18):

$$\int_\Gamma \left[\Lambda_1 \nabla_{\Lambda,1} u_{h,1} \cdot \boldsymbol{n}_1 + \alpha_{12}\Phi_1(u_{h,1})\right] \Phi_1(v_{h,1}^Q) d\gamma$$
$$= \int_\Gamma \left[\Lambda_2 \nabla_{\Lambda,2} u_{h,2} \cdot \boldsymbol{n}_1 + \alpha_{12}\Phi_2(u_{h,2})\right] \Phi_2(v_{h,2}^Q) d\gamma, \quad \forall Q \in \mathcal{N}_{\Gamma,\circ}^{**}, \tag{3.27a}$$
$$\int_\Gamma \left[\Lambda_1 \nabla_{\Lambda,1} u_{h,1} \cdot \boldsymbol{n}_1 + \alpha_{12}\Phi_1(u_{h,1})\right] \Phi_1(v_{h,1}^{Q_1}) d\gamma$$
$$= \int_\Gamma \left[\Lambda_2 \nabla_{\Lambda,2} u_{h,2} \cdot \boldsymbol{n}_1 + \alpha_{12}\Phi_2(u_{h,2})\right] \Phi_2\left(E_{h,2}(v_{1,\Gamma}^{Q_1})\right) d\gamma, \quad \forall Q_1 \in \mathcal{C}_1^\Gamma, \tag{3.27b}$$

and similarly for (3.23),

$$\int_\Gamma \left[\Lambda_2 \nabla_{\Lambda,2} u_{h,2} \cdot \boldsymbol{n}_2 + \alpha_{21}\Phi_2(u_{h,2})\right] \Phi_2(v_{h,2}^Q) d\gamma$$
$$= \int_\Gamma \left[\Lambda_1 \nabla_{\Lambda,1} u_{h,1} \cdot \boldsymbol{n}_2 + \alpha_{21}\Phi_1(u_{h,1})\right] \Phi_1(v_{h,1}^Q) d\gamma, \quad \forall Q \in \mathcal{N}_{\Gamma,\circ}^{**}, \tag{3.28a}$$
$$\int_\Gamma \left[\Lambda_2 \nabla_{\Lambda,2} u_{h,2} \cdot \boldsymbol{n}_2 + \alpha_{21}\Phi_2(u_{h,2})\right] \Phi_2(v_{h,2}^{Q_2}) d\gamma$$
$$= \int_\Gamma \left[\Lambda_1 \nabla_{\Lambda,1} u_{h,1} \cdot \boldsymbol{n}_2 + \alpha_{21}\Phi_1(u_{h,1})\right] \Phi_1\left(E_{h,1}(v_{2,\Gamma}^{Q_2})\right) d\gamma, \quad \forall Q_2 \in \mathcal{C}_2^\Gamma. \tag{3.28b}$$

Finally, we combine linearly the two equations (3.20) and (3.21) using the parameters α_{12} and α_{21}:

$$\int_e \left(\Lambda_1 \nabla_{\Lambda,1} u_{h,1} \cdot \boldsymbol{n}_1 + \alpha_{12} u_{1,\sigma}^M\right) d\gamma = \int_e \left(\Lambda_2 \nabla_{\Lambda,2} u_{h,2} \cdot \boldsymbol{n}_1 + \alpha_{12} u_{2,\sigma}^M\right) d\gamma, \tag{3.29a}$$
$$\int_e \left(\Lambda_2 \nabla_{\Lambda,2} u_{h,2} \cdot \boldsymbol{n}_2 + \alpha_{21} u_{2,\sigma}^M\right) d\gamma = \int_e \left(\Lambda_1 \nabla_{\Lambda,1} u_{h,1} \cdot \boldsymbol{n}_2 + \alpha_{21} u_{1,\sigma}^M\right) d\gamma, \tag{3.29b}$$

for all $e = C_M C_\sigma \in \mathcal{E}_\Gamma^{**}$, $C_M \in \mathcal{N}_{\Gamma,\circ}^{**}$, $C_\sigma \in \mathcal{N}_{\Gamma,\square}^{**}$. One can easily prove that the equations (3.29a)-(3.29b) are equivalent to (3.20)-(3.21).

We now derive the interface problem corresponding to the new Robin-type transmission conditions (3.27)-(3.29): for a given function $\zeta_{h,i} \in \mathcal{G}_h$ and a given vector $\theta_{h,i} = \left(\theta_{h,i}^e\right)_{e \in \mathcal{E}_\Gamma^{**}}$, we denote by $u_{h,i}(\zeta_{h,i}, \theta_{h,i}, f_i)$, $i = 1, 2$, the solution of the subdomain problem with Robin boundary conditions on the interface:

Find $u_{h,i} \in X_{h,i}^{0,\partial\Omega_i \cap \partial\Omega}$ such that :

$$\int_{\Omega_i} (\Lambda_i \nabla_{\Lambda,i} u_{h,i}) \cdot \nabla_{\Lambda,i} v_{h,i}\, d\boldsymbol{x} - \int_\Gamma (\Lambda_i \nabla_{\Lambda,i} u_{h,i}) \cdot \boldsymbol{n}_i \Phi_i(v_{h,i}) d\gamma = \int_{\Omega_i} f_i \Phi_i(v_{h,i})\, d\boldsymbol{x},$$
$$\forall v_{h,i} \in X_{h,i}^{0,\partial\Omega_i \cap \partial\Omega}, \tag{3.30}$$
$$\int_\Gamma \left[\Lambda_i \nabla_{\Lambda,i} u_{h,i} \cdot \boldsymbol{n}_i + \alpha_{ij}\Phi_i(u_{h,i})\right] \Phi_i(v_{h,i}^Q)\, d\gamma = \int_\Gamma \zeta_{h,i} \Phi_i(v_{h,i}^Q)\, d\gamma, \ \forall Q \in \mathcal{N}_{\Gamma,\circ}^{**} \cup \mathcal{C}_i^\Gamma, \tag{3.31}$$
$$\int_e \left(\Lambda_i \nabla_{\Lambda,i} u_{h,i} \cdot \boldsymbol{n}_i + \alpha_{ij} u_{i,\sigma}^M\right) d\gamma = \theta_{h,i}^e, \ \forall e = C_M C_\sigma \in \mathcal{E}_\Gamma^{**}. \tag{3.32}$$

Then the interface problem associated with (3.27) -(3.29) is:

$$\begin{cases} \displaystyle\int_\Gamma \zeta_{h,i}\Phi_i(v_{h,i}^Q)\,d\gamma - \int_\Gamma \left[\begin{array}{l} \Lambda_j\nabla_{\Lambda,j}u_{h,j}(\zeta_{h,j},\theta_{h,j},f_j)\cdot\boldsymbol{n}_i + \\ \alpha_{ij}\Phi_j(u_{h,j}(\zeta_{h,j},\theta_{h,j},f_j)) \end{array}\right]\Phi_j(v_{h,j}^Q)\,d\gamma = 0,\ \forall Q\in\mathcal{N}_{\Gamma,\mathrm{o}}^{**}, \\ \displaystyle\int_\Gamma \zeta_{h,i}\Phi_i(v_{h,i}^Q)\,d\gamma - \int_\Gamma \left[\begin{array}{l} \Lambda_j\nabla_{\Lambda,j}u_{h,j}(\zeta_{h,j},\theta_{h,j},f_j)\cdot\boldsymbol{n}_i + \\ \alpha_{ij}\Phi_j(u_{h,j}(\zeta_{h,j},\theta_{h,j},f_j)) \end{array}\right]\Phi_j\left(E_{h,j}(v_{i,\Gamma}^Q)\right)\,d\gamma = 0,\ \forall Q\in\mathcal{C}_i^\Gamma, \\ \theta_{h,i}^e - \displaystyle\int_e \left(\Lambda_j\nabla_{\Lambda,j}u_{h,j}(\zeta_{h,j},\theta_{h,j},f_j)\cdot\boldsymbol{n}_i + \alpha_{ij}u_{j,\sigma}^M(\zeta_{h,j},\theta_{h,j},f_j)\right)\,d\gamma = 0,\ \forall e = C_MC_\sigma\in\mathcal{E}_\Gamma^{**}. \end{cases} \tag{3.33}$$

for $i = 1, 2$, and $j = (3 - i)$.

This problem can be transformed into a system of equations in which the left hand side depends only on the interface unknowns $(\zeta_{h,1}, \theta_{h,1}, \zeta_{h,2}, \theta_{h,2})$. Such a system is then solved iteratively using Jacobi method or GMRES. The former choice leads to the following Robin-to-Robin algorithm.

3.3. Robin-to-Robin algorithm and convergence analysis

The derivation of the interface problem (3.33) with Robin transmission conditions can be extended straightforwardly to the case of many strip-shaped subdomains. In particular, we decompose the domain Ω into N nonoverlapping subdomains $\{\Omega_i\}_{1\le i\le N}$ aligned in the same direction: $\overline{\Omega} = \cup_{i=1}^N\overline{\Omega}_i$. Let $\Gamma_{ij} = \partial\Omega_i\cap\partial\Omega_j$, $i\neq j$ be the interfaces between subdomains. Similar notation as introduced in Subsection 3.1 for the interface Γ is used for the interfaces $\Gamma_{ij}\neq\emptyset$ between the neighboring strips Ω_i and Ω_j.

The Robin-to-Robin algorithm reads as follows: *For given initial guesses*

$$g_{ij} = \left(\Lambda_j\nabla_{\Lambda,j}u_{h,j}^0\cdot\boldsymbol{n}_i + \alpha_{ij}\Phi_j(u_{h,j}^0)\right)|_{\Gamma_{ij}},\ \textit{and}\ \widehat{g}_{ij} = \left(\Lambda_j\nabla_{\Lambda,j}u_{h,j}^0\cdot\boldsymbol{n}_i + \alpha_{ij}u_{j,\sigma}^{Q,0}\right)|_{e=QC_\sigma\in\mathcal{E}_{\Gamma_{ij}}^{**}},$$

at the $(n+1)-$th iteration, solve in each subdomain the following problem:

Find $u_{h,i}^{n+1}\in X_{h,i}^{0,\partial\Omega_i\cap\partial\Omega}$ *such that*:

$$\int_{\Omega_i}\left(\Lambda_i\nabla_{\Lambda,i}u_{h,i}^{n+1}\right)\cdot\nabla_{\Lambda,i}v_{h,i}\,d\boldsymbol{x} - \sum_{\substack{j\\ \Gamma_{ij}\neq\emptyset}}\int_{\Gamma_{ij}}(\Lambda_i\nabla_{\Lambda,i}u_{h,i}^{n+1})\cdot\boldsymbol{n}_i\Phi_i(v_{h,i})d\gamma = \int_{\Omega_i}f_i\Phi_i(v_{h,i})\,d\boldsymbol{x},$$
$$\forall v_{h,i}\in X_{h,i}^{0,\partial\Omega_i\cap\partial\Omega}, \tag{3.34}$$

together with Robin boundary conditions given by the neighboring subdomains at the previous iteration: for all j that $\Gamma_{ij}\neq\emptyset$

$$\sum_{e\in\mathcal{E}^{**}_{\Gamma_{ij}}}\int_e\left[\Lambda_i\nabla_{\Lambda,i}u^{n+1}_{h,i}\cdot\boldsymbol{n}_i+\alpha_{ij}\Phi_i\left(u^{n+1}_{h,i}\right)\right]\Phi_i\left(v^{Q}_{h,i}\right)d\gamma$$

$$=\sum_{e\in\mathcal{E}^{**}_{\Gamma_{ij}}}\int_e\left[\Lambda_j\nabla_{\Lambda,j}u^{n}_{h,j}\cdot\boldsymbol{n}_i+\alpha_{ij}\Phi_j\left(u^{n}_{h,j}\right)\right]\Phi_j\left(v^{Q}_{h,j}\right)d\gamma,\quad\forall Q\in\mathcal{N}^{**}_{\Gamma_{ij},\circ},\tag{3.35}$$

$$\sum_{e\in\mathcal{E}^{**}_{\Gamma_{ij}}}\int_e\left[\Lambda_i\nabla_{\Lambda,i}u^{n+1}_{h,i}\cdot\boldsymbol{n}_i+\alpha_{ij}\Phi_i\left(u^{n+1}_{h,i}\right)\right]\Phi_i\left(v^{Q_i}_{h,i}\right)d\gamma$$

$$=\sum_{e\in\mathcal{E}^{**}_{\Gamma_{ij}}}\int_e\left[\Lambda_j\nabla_{\Lambda,j}u^{n}_{h,j}\cdot\boldsymbol{n}_i+\alpha_{ij}\Phi_j(u^{n}_{h,j})\right]\Phi_j\left(E_{h,j}(v^{Q_i}_{i,\Gamma_{ij}})\right)d\gamma,\quad\forall Q_i\in\mathcal{C}_i^{\Gamma_{ij}},\tag{3.36}$$

$$\int_e\left(\Lambda_i\nabla_{\Lambda,i}u^{n+1}_{h,i}\cdot\boldsymbol{n}_i+\alpha_{ij}u^{Q,n+1}_{i,\sigma}\right)d\gamma=\int_e\left(\Lambda_j\nabla_{\Lambda,j}u^{n}_{h,j}\cdot\boldsymbol{n}_i+\alpha_{ij}u^{Q,n}_{j,\sigma}\right)d\gamma,$$
$$\forall e=QC_\sigma\in\mathcal{E}^{**}_{\Gamma_{ij}},\ \textit{with}\ Q\in\mathcal{N}^{**}_{\Gamma_{ij},\circ},C_\sigma\in\mathcal{N}^{**}_{\Gamma_{ij},\square}.\tag{3.37}$$

For convergence analysis, we assume that the coefficients of the Robin conditions satisfy:

$$\alpha_{ij}=\alpha_{ji}\geq\alpha>0\quad\text{for } i,j=1,...,N \text{ and } i\neq j.\tag{3.38}$$

Numerical results with both equal and different Robin parameters will be discussed in Section 4. The convergence of the Robin-to-Robin algorithm is guaranteed by the following theorem.

Theorem 3.1. *Under assumption* (3.38)*, the Robin-to-Robin algorithm converges. In particular, we have:*

$$\lim_{n\to\infty}\sum_{i=1}^{N}\int_{\Omega_i}\left[\Lambda_i\nabla_{\Lambda,i}\left(u^n_{h,i}-u_{h,i}\right)\right]\cdot\nabla_{\Lambda,i}\left(u^n_{h,i}-u_{h,i}\right)d\boldsymbol{x}=0,\quad\textit{for } i=1,\ldots,N,\tag{3.39}$$

where $u_{h,i}$ is the restriction of the solution u_h to Ω_i and N is the number of subdomains.

Proof. Denote by $\varepsilon^n_{h,i}=u^n_{h,i}-u_{h,i}$, the error between the iterative solution and the monodomain solution. Then by using the Robin transmission conditions (3.35)-(3.37) and integration by parts, we obtain:

$$\int_{\Omega_i}\left(\Lambda_i\nabla_{\Lambda,i}\varepsilon_{h,i}^{n+1}\right)\cdot\nabla_{\Lambda,i}v_{h,i}^{Q}\,d\boldsymbol{x}+\sum_{\substack{j\\ \Gamma_{ij}\neq\emptyset}}\sum_{e\in\mathcal{E}_{\Gamma_{ij}}^{**}}\int_e\alpha_{ij}\Phi_i\left(\varepsilon_{h,i}^{n+1}\right)\,\Phi_i(v_{h,i}^{Q})\,d\gamma$$

$$=\sum_{\substack{j\\ \Gamma_{ij}\neq\emptyset}}\sum_{e\in\mathcal{E}_{\Gamma_{ij}}^{**}}\int_e\left[\Lambda_j\nabla_{\Lambda,j}\varepsilon_{h,j}^{n}\cdot\boldsymbol{n}_i+\alpha_{ij}\Phi_j\left(\varepsilon_{h,j}^{n}\right)\right]\Phi_j\left(v_{h,j}^{Q}\right)\,d\gamma,\quad\forall Q\in\mathcal{N}_{\Gamma_{ij},\circ}^{**},\tag{3.40a}$$

$$\int_{\Omega_i}\left(\Lambda_i\nabla_{\Lambda,i}\varepsilon_{h,i}^{n+1}\right)\cdot\nabla_{\Lambda,i}v_{h,i}^{Q_i}\,d\boldsymbol{x}+\sum_{\substack{j\\ \Gamma_{ij}\neq\emptyset}}\sum_{e\in\mathcal{E}_{\Gamma_{ij}}^{**}}\int_e\alpha_{ij}\Phi_i\left(\varepsilon_{h,i}^{n+1}\right)\,\Phi_i(v_{h,i}^{Q_i})\,d\gamma$$

$$=\sum_{\substack{j\\ \Gamma_{ij}\neq\emptyset}}\sum_{e\in\mathcal{E}_{\Gamma_{ij}}^{**}}\int_e\left[\Lambda_j\nabla_{\Lambda,j}\varepsilon_{h,j}^{n}\cdot\boldsymbol{n}_i+\alpha_{ij}\Phi_j\left(\varepsilon_{h,j}^{n}\right)\right]\Phi_j\left(E_{h,j}(v_{i,\Gamma_{ij}}^{Q_i})\right)\,d\gamma,\ \forall Q_i\in\mathcal{C}_i^{\Gamma_{ij}},\tag{3.40b}$$

$$\int_{\Omega_i}\left[\Lambda_i\nabla_{\Lambda,i}\varepsilon_{h,i}^{n+1}\right]\cdot\nabla_{\Lambda,i}v_{h,i}^{M}\,d\boldsymbol{x}=0,\quad\forall M\in(\mathcal{C}_i\cup\mathcal{C}_i^{*})\setminus\mathcal{C}_i^{\Gamma_{ij}}.\tag{3.40c}$$

From which, we deduce, for $v_{h,i}\in X_{h,i}^{0,\partial\Omega_i\cap\partial\Omega}$, that

$$\int_{\Omega_i}\left(\Lambda_i\nabla_{\Lambda,i}\varepsilon_{h,i}^{n+1}\right)\cdot\nabla_{\Lambda,i}v_{h,i}\,d\boldsymbol{x}+\sum_{\substack{j\\ \Gamma_{ij}\neq\emptyset}}\sum_{e\in\mathcal{E}_{\Gamma_{ij}}^{**}}\int_e\alpha_{ij}\Phi_i\left(\varepsilon_{h,i}^{n+1}\right)\,\Phi_i\left(v_{h,i}\right)\,d\gamma$$

$$=\sum_{\substack{j\\ \Gamma_{ij}\neq\emptyset}}\sum_{e\in\mathcal{E}_{\Gamma_{ij}}^{**}}\int_e\left[\Lambda_j\nabla_{\Lambda,j}\varepsilon_{h,j}^{n}\cdot\boldsymbol{n}_{ij}+\alpha_{ij}\Phi_j\left(\varepsilon_{h,j}^{n}\right)\right]\Phi_j\left(E_{h,j}(v_{i,\Gamma_{ij}})\right)\,d\gamma.\tag{3.41}$$

where $v_{i,\Gamma_{ij}}=(v_{i,P})_{P\in\mathcal{N}_{\Gamma_{ij}}^{**}}$ is a vector consisting of unknowns on the interface Γ_{ij}, and the extension operator $E_{h,j}$ is defined similarly to (3.15). Equation (3.41) can be rewritten equivalently as:

$$\int_{\Omega_i}\left(\Lambda_i\nabla_{\Lambda,i}\varepsilon_{h,i}^{n+1}\right)\cdot\nabla_{\Lambda,i}v_{h,i}\,d\boldsymbol{x}-\sum_{\substack{j\\ \Gamma_{ij}\neq\emptyset}}\sum_{e\in\mathcal{E}_{\Gamma_{ij}}^{**}}\int_e\Lambda_i\nabla_{\Lambda,i}\varepsilon_{h,i}^{n+1}\cdot\boldsymbol{n}_{ij}\Phi_i\left(v_{h,i}\right)d\gamma$$

$$=\sum_{\substack{j\\ \Gamma_{ij}\neq\emptyset}}\sum_{e\in\mathcal{E}_{\Gamma_{ij}}^{**}}\int_e\left[\begin{array}{l}\left(\Lambda_j\nabla_{\Lambda,j}\varepsilon_{h,j}^{n}\cdot\boldsymbol{n}_{ij}+\alpha_{ij}\Phi_j\left(\varepsilon_{h,j}^{n}\right)\right)\Phi_j\left(E_{h,j}(v_{i,\Gamma_{ij}})\right)\\ -\left(\Lambda_i\nabla_{\Lambda,i}\varepsilon_{h,i}^{n+1}\cdot\boldsymbol{n}_{ij}+\alpha_{ij}\Phi_i\left(\varepsilon_{h,i}^{n+1}\right)\right)\Phi_i\left(v_{h,i}\right)\end{array}\right]d\gamma,\quad\forall v_{h,i}\in X_{h,i}^{0,\partial\Omega_i\cap\partial\Omega}.\tag{3.42}$$

Note that on the one hand, by the Robin transmission conditions on the interfaces between the subdomains, we have:

$$\sum_{\substack{j\\ \Gamma_{ij}\neq\emptyset}}\sum_{e\in\mathcal{E}_{\Gamma_{ij}}^{**}}\int_e\left[\begin{array}{l}\left(\Lambda_j\nabla_{\Lambda,j}u_{h,j}^{n}\cdot\boldsymbol{n}_{ij}+\alpha_{ij}\Phi_j\left(u_{h,j}^{n}\right)\right)\Phi_j\left(E_{h,j}(v_{i,\Gamma_{ij}})\right)\\ -\left(\Lambda_i\nabla_{\Lambda,i}u_{h,i}^{n+1}\cdot\boldsymbol{n}_{ij}+\alpha_{ij}\Phi_i\left(u_{h,i}^{n+1}\right)\right)\Phi_i\left(v_{h,i}\right)\end{array}\right]d\gamma=0,\quad\forall v_{h,i}\in X_{h,i}^{0,\partial\Omega_i\cap\partial\Omega}.\tag{3.43}$$

On the other hand, by construction (cf. Equations (3.27) and (3.28)), the monodomain solution satisfies

$$\sum_{\substack{j\\ \Gamma_{ij}\neq\emptyset}}\sum_{e\in\mathcal{E}^{**}_{\Gamma_{ij}}}\int_e\left[\begin{array}{l}\left(\Lambda_j\nabla_{\Lambda,j}u_{h,j}\cdot\boldsymbol{n}_{ij}+\alpha_{ij}\Phi_j\left(u_{h,j}\right)\right)\Phi_j\left(E_{h,j}(v_{i,\Gamma_{ij}})\right)\\ -\left(\Lambda_i\nabla_{\Lambda,i}u_{h,i}\cdot\boldsymbol{n}_{ij}+\alpha_{ij}\Phi_i\left(u_{h,i}\right)\right)\Phi_i\left(v_{h,i}\right)\end{array}\right]d\gamma=0,\quad\forall v_{h,i}\in X^{0,\partial\Omega_i\cap\partial\Omega}_{h,i}.\tag{3.44}$$

Therefore, combining (3.43) and (3.44) yields

$$\sum_{\substack{j\\ \Gamma_{ij}\neq\emptyset}}\sum_{e\in\mathcal{E}^{**}_{\Gamma_{ij}}}\int_e\left[\begin{array}{l}\left(\Lambda_j\nabla_{\Lambda,j}\varepsilon^n_{h,j}\cdot\boldsymbol{n}_{ij}+\alpha_{ij}\Phi_j\left(\varepsilon^n_{h,j}\right)\right)\Phi_j\left(E_{h,j}(v_{i,\Gamma_{ij}})\right)\\ -\left(\Lambda_i\nabla_{\Lambda,i}\varepsilon^{n+1}_{h,i}\cdot\boldsymbol{n}_{ij}+\alpha_{ij}\Phi_i\left(\varepsilon^{n+1}_{h,i}\right)\right)\Phi_i\left(v_{h,i}\right)\end{array}\right]d\gamma=0,\quad\forall v_{h,i}\in X^{0,\partial\Omega_i\cap\partial\Omega}_{h,i}.\tag{3.45}$$

Substituting this into (3.42), and choosing $v_{h,i}=\varepsilon^{n+1}_{h,i}$, we obtain

$$\int_{\Omega_i}\left(\Lambda_i\nabla_{\Lambda,i}\varepsilon^{n+1}_{h,i}\right)\cdot\nabla_{\Lambda,i}\varepsilon^{n+1}_{h,i}\,d\boldsymbol{x}-\sum_{j,\Gamma_{ij}\neq\emptyset}\sum_{e\in\mathcal{E}^{**}_{\Gamma_{ij}}}\int_e\left(\Lambda_i\nabla_{\Lambda,i}\varepsilon^{n+1}_{h,i}\cdot\boldsymbol{n}_{ij}\right)\Phi_i\left(\varepsilon^{n+1}_{h,i}\right)d\gamma=0.\tag{3.46}$$

Next, we use the identity

$$(a+\lambda_1 b)^2-(a-\lambda_2 b)^2=2(\lambda_1+\lambda_2)ab+(\lambda_1^2-\lambda_2^2)b^2,$$

to write the second term in (3.46) as follows:

$$\begin{aligned}-\sum_{e\in\mathcal{E}^{**}_{\Gamma_{ij}}}\int_e\left(\Lambda_i\nabla_{\Lambda,i}\varepsilon^{n+1}_{h,i}\cdot\boldsymbol{n}_{ij}\right)\Phi_i(\varepsilon^{n+1}_{h,i})d\gamma=&\frac{1}{4\alpha_{ij}}\sum_{e\in\mathcal{E}^{**}_{\Gamma_{ij}}}\int_e\left[\Lambda_i\nabla_{\Lambda,i}\varepsilon^{n+1}_{h,i}\cdot\boldsymbol{n}_{ij}-\alpha_{ij}\Phi_i(\varepsilon^{n+1}_{h,i})\right]^2d\gamma\\&-\frac{1}{4\alpha_{ij}}\sum_{e\in\mathcal{E}^{**}_{\Gamma_{ij}}}\int_e\left[\Lambda_i\nabla_{\Lambda,i}\varepsilon^{n+1}_{h,i}\cdot\boldsymbol{n}_{ij}+\alpha_{ij}\Phi_i(\varepsilon^{n+1}_{h,i})\right]^2d\gamma,\end{aligned}$$

Substituting this into (3.46), we find that

$$\begin{aligned}\int_{\Omega_i}\left(\Lambda_i\nabla_{\Lambda,i}\varepsilon^{n+1}_{h,i}\right)\cdot\nabla_{\Lambda,i}\varepsilon^{n+1}_{h,i}dx+\frac{1}{4\alpha_{ij}}\sum_{e\in\mathcal{E}^{**}_{\Gamma_{ij}}}\int_e\left[\Lambda_i\nabla_{\Lambda,i}\varepsilon^{n+1}_{h,i}\cdot\boldsymbol{n}_{ij}-\alpha_{ij}\Phi_i(\varepsilon^{n+1}_{h,i})\right]^2d\gamma\\=\frac{1}{4\alpha_{ij}}\sum_{e\in\mathcal{E}^{**}_{\Gamma_{ij}}}\int_e\left[\Lambda_i\nabla_{\Lambda,i}\varepsilon^{n+1}_{h,i}\cdot\boldsymbol{n}_{ij}+\alpha_{ij}\Phi_i(\varepsilon^{n+1}_{h,i})\right]^2d\gamma,\end{aligned}\tag{3.47}$$

or equivalently in a compact form,

$$A_{i,n+1} + \frac{1}{4\alpha_{ij}} B^{(1)}_{ij,n+1} = \frac{1}{4\alpha_{ij}} B^{(2)}_{ij,n+1}, \quad \text{for } i,j = 1,...,N, \text{ and } i \neq j, \tag{3.48}$$

where

$$A_{i,n+1} = \int_{\Omega_i} \left(\Lambda_i \nabla_{\Lambda,i} \varepsilon^{n+1}_{h,i} \right) \cdot \nabla_{\Lambda,i} \varepsilon^{n+1}_{h,i} d\boldsymbol{x}$$

$$B^{(1)}_{ij,n+1} = \sum_{e \in \mathcal{E}^{**}_{\Gamma_{ij}}} \int_e \left[\Lambda_i \nabla_{\Lambda,i} \varepsilon^{n+1}_{h,i} \cdot \boldsymbol{n}_{ij} - \alpha_{ij} \Phi_i(\varepsilon^{n+1}_{h,i}) \right]^2 d\gamma$$

$$B^{(2)}_{ij,n+1} = \sum_{e \in \mathcal{E}^{**}_{\Gamma_{ij}}} \int_e \left[\Lambda_i \nabla_{\Lambda,i} \varepsilon^{n+1}_{h,i} \cdot \boldsymbol{n}_{ij} + \alpha_{ij} \Phi_i(\varepsilon^{n+1}_{h,i}) \right]^2 d\gamma.$$

We shall show that $B^{(2)}_{ij,n+1} = B^{(1)}_{ji,n}$. For that purpose, we first prove, for all $Q \in \mathcal{N}^{**}_{\Gamma_{ij},\circ} \cup \mathcal{C}_i^{\Gamma_{ij}}$, that:

$$\sum_{e \in \mathcal{E}^{**}_{\Gamma_{ij}}} \int_e \left(\Lambda_i \nabla_{\Lambda,i} \varepsilon^{n+1}_{h,i} \cdot \boldsymbol{n}_{ij} + \alpha_{ij} \varepsilon^{n+1}_{i,Q} \right) d\gamma = \sum_{e \in \mathcal{E}^{**}_{\Gamma_{ij}}} \int_e \left(\Lambda_j \nabla_{\Lambda,j} \varepsilon^{n}_{h,j} \cdot \boldsymbol{n}_{ij} + \alpha_{ij} \varepsilon^{n}_{j,Q} \right) d\gamma, \tag{3.49}$$

or equivalently

$$\sum_{e \in \mathcal{E}^{**}_{\Gamma_{ij}}} \int_e \left(\Lambda_i \nabla_{\Lambda,i} u^{n+1}_{h,i} \cdot \boldsymbol{n}_{ij} + \alpha_{ij} u^{n+1}_{i,Q} \right) d\gamma = \sum_{e \in \mathcal{E}^{**}_{\Gamma_{ij}}} \int_e \left(\Lambda_j \nabla_{\Lambda,j} u^{n}_{h,j} \cdot \boldsymbol{n}_{ij} + \alpha_{ij} u^{n}_{j,Q} \right) d\gamma. \tag{3.50}$$

We consider two cases as depicted in Figure 5:

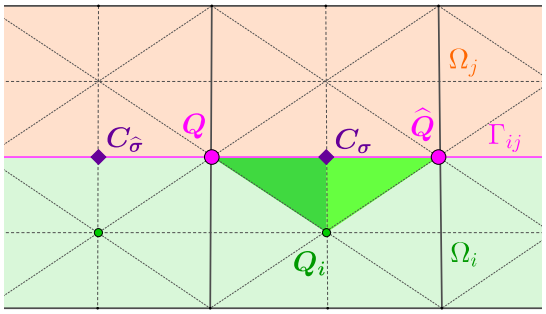

Figure 5: Examples of the point $Q \in \mathcal{N}^{**}_{\Gamma_{ij},\circ}$ (Case 1) and $Q_i \in \mathcal{C}_i^{\Gamma_{ij}}$ (Case 2).

(i) Case 1: $Q \in \mathcal{N}^{**}_{\Gamma_{ij},\circ}$. We shall compute the integrals in the Robin transmission condition (3.35) exactly. Note that by construction, the restriction of

$$\left(\Lambda_j \nabla_{\Lambda,j} u^n_{h,j} \cdot \boldsymbol{n}_{ij} + \alpha_{ij} \Phi_j \left(u^n_{h,j} \right) \right) \Phi_j \left(v^Q_{h,j} \right) \text{ and } \left(\Lambda_i \nabla_{\Lambda,i} u^{n+1}_{h,i} \cdot \boldsymbol{n}_{ij} + \alpha_{ij} \Phi_i \left(u^{n+1}_{h,i} \right) \right) \Phi_i \left(v^Q_{h,i} \right),$$

to Γ_{ij} are piecewise continuous polynomials of order 2 and are nonzero only on $e = QC_\sigma$ and $\widehat{e} = QC_{\widehat{\sigma}}$ (see Figure 5). Denote by $\mathcal{E}^{**}_{\Gamma_{ij}}(Q) = \{QC_\sigma, QC_{\widehat{\sigma}}\}$. By using the Simpson's rule, the integrals in (3.35) are computed as follows:

$$\begin{aligned}
&\sum_{e\in\mathcal{E}^{**}_{\Gamma_{ij}}} \int_e \left[\Lambda_i \nabla_{\Lambda,i} u^{n+1}_{h,i} \cdot \boldsymbol{n}_{ij} + \alpha_{ij}\Phi_i\left(u^{n+1}_{h,i}\right)\right]\Phi_i\left(v^Q_{h,i}\right)\, d\gamma \\
&= \sum_{\substack{e\in\mathcal{E}^{**}_{\Gamma_{ij}}(Q)\\ e=QC_\sigma}} \int_e \left[\Lambda_i \nabla_{\Lambda,i} u^{n+1}_{h,i} \cdot \boldsymbol{n}_{ij} + \alpha_{ij}\Phi_i\left(u^{n+1}_{h,i}\right)\right]\Phi_i\left(v^Q_{h,i}\right)\, d\gamma \\
&= \sum_{\substack{e\in\mathcal{E}^{**}_{\Gamma_{ij}}(Q)\\ e=QC_\sigma}} \frac{|e|}{6}\left\{\begin{array}{l}
\left[\Lambda_i \nabla_{\Lambda,i} u^{n+1}_{h,i} \cdot \boldsymbol{n}_{ij}|_e + \alpha_{ij}\Phi_i\left(u^{n+1}_{h,i}\right)(\boldsymbol{x}_Q)\right]\Phi_i\left(v^Q_{h,i}\right)(\boldsymbol{x}_Q) + \\
\left[\Lambda_i \nabla_{\Lambda,i} u^{n+1}_{h,i} \cdot \boldsymbol{n}_{ij}|_e + \alpha_{ij}\Phi_i\left(u^{n+1}_{h,i}\right)(\boldsymbol{x}_{C_\sigma})\right]\Phi_i\left(v^Q_{h,i}\right)(\boldsymbol{x}_{C_\sigma}) + \\
4\left[\Lambda_i \nabla_{\Lambda,i} u^{n+1}_{h,i} \cdot \boldsymbol{n}_{ij}|_e + \alpha_{ij}\Phi_i\left(u^{n+1}_{h,i}\right)\left(\frac{\boldsymbol{x}_Q+\boldsymbol{x}_{C_\sigma}}{2}\right)\right]\Phi_i\left(v^Q_{h,i}\right)\left(\frac{\boldsymbol{x}_Q+\boldsymbol{x}_{C_\sigma}}{2}\right)
\end{array}\right\}.
\end{aligned} \tag{3.51}$$

As the projection operator Φ_i is linear, and by the definition of the test function, we have

$$\Phi_i\left(v^Q_{h,i}\right)\left(\frac{\boldsymbol{x}_Q+\boldsymbol{x}_{C_\sigma}}{2}\right) = \frac{1}{2}\left[\Phi_i\left(v^Q_{h,i}\right)(\boldsymbol{x}_Q) + \Phi_i\left(v^Q_{h,i}\right)(\boldsymbol{x}_{C_\sigma})\right] = \frac{1}{2}\left(1 + v^Q_{i,\sigma}\right),$$

where $v^Q_{i,\sigma} = \Phi_i\left(v^Q_{h,i}\right)(\boldsymbol{x}_{C_\sigma})$. Substituting this into (3.51), we obtain:

$$\begin{aligned}
&\sum_{e\in\mathcal{E}^{**}_{\Gamma_{ij}}} \int_e \left[\Lambda_i \nabla_{\Lambda,i} u^{n+1}_{h,i} \cdot \boldsymbol{n}_{ij} + \alpha_{ij}\Phi_i\left(u^{n+1}_{h,i}\right)\right]\Phi_i\left(v^Q_{h,i}\right)\, d\gamma \\
&= \sum_{\substack{e\in\mathcal{E}^{**}_{\Gamma_{ij}}(Q)\\ e=QC_\sigma}} \frac{|e|}{6}\left\{\begin{array}{l}
\left[\Lambda_i \nabla_{\Lambda,i} u^{n+1}_{h,i} \cdot \boldsymbol{n}_{ij}|_e + \alpha_{ij} u^{n+1}_{i,Q}\right] + \\
\left[\Lambda_i \nabla_{\Lambda,i} u^{n+1}_{h,i} \cdot \boldsymbol{n}_{ij}|_e + \alpha_{ij} u^{Q,n+1}_{i,\sigma}\right] v^Q_{i,\sigma} + \\
\left[\begin{array}{l}\Lambda_i \nabla_{\Lambda,i} u^{n+1}_{h,i} \cdot \boldsymbol{n}_{ij}|_e + \alpha_{ij} u^{n+1}_{i,Q} + \\ \Lambda_i \nabla_{\Lambda,i} u^{n+1}_{h,i} \cdot \boldsymbol{n}_{ij}|_e + \alpha_{ij} u^{Q,n+1}_{i,\sigma}\end{array}\right]\left(1 + v^Q_{i,\sigma}\right)
\end{array}\right\},
\end{aligned}$$

or

$$\begin{aligned}
&\sum_{e\in\mathcal{E}^{**}_{\Gamma_{ij}}} \int_e \left[\Lambda_i \nabla_{\Lambda,i} u^{n+1}_{h,i} \cdot \boldsymbol{n}_{ij} + \alpha_{ij}\Phi_i\left(u^{n+1}_{h,i}\right)\right]\Phi_i\left(v^Q_{h,i}\right)\, d\gamma \\
&= \sum_{\substack{e\in\mathcal{E}^{**}_{\Gamma_{ij}}(Q)\\ e=QC_\sigma}} \frac{1}{6}\left\{\begin{array}{l}
\left(2 + v^Q_{i,\sigma}\right)\displaystyle\int_e \left[\Lambda_i \nabla_{\Lambda,i} u^{n+1}_{h,i} \cdot \boldsymbol{n}_{ij} + \alpha_{ij} u^{n+1}_{i,Q}\right] d\gamma + \\
\left(1 + 2v^Q_{i,\sigma}\right)\displaystyle\int_e \left[\Lambda_i \nabla_{\Lambda,i} u^{n+1}_{h,i} \cdot \boldsymbol{n}_{ij} + \alpha_{ij} u^{Q,n+1}_{i,\sigma}\right] d\gamma
\end{array}\right\}.
\end{aligned} \tag{3.52}$$

Similar calculations yield:

$$\sum_{e\in\mathcal{E}^{**}_{\Gamma_{ij}}}\int_e\left[\Lambda_j\nabla_{\Lambda,j}u^n_{h,j}\cdot\boldsymbol{n}_{ij}+\alpha_{ij}\Phi_j(u^n_{h,j})\right]\Phi_j\left(v^Q_{h,j}\right)\,d\gamma$$

$$=\sum_{\substack{e\in\mathcal{E}^{**}_{\Gamma_{ij}}(Q)\\ e=QC_\sigma\in\sigma}}\frac{1}{6}\left\{\begin{array}{l}\left(2+v^Q_{i,\sigma}\right)\displaystyle\int_e\left[\Lambda_j\nabla_{\Lambda,j}u^n_{h,j}\cdot\boldsymbol{n}_{ij}+\alpha_{ij}u^n_{j,Q}\right]d\gamma+\\ \left(1+2v^Q_{i,\sigma}\right)\displaystyle\int_e\left[\Lambda_j\nabla_{\Lambda,j}u^n_{h,j}\cdot\boldsymbol{n}_{ij}+\alpha_{ij}u^{Q,n}_{j,\sigma}\right]d\gamma\end{array}\right\}. \tag{3.53}$$

Thus, by combining (3.35), (3.37), (3.52) and (3.53), we deduce that (3.50) holds for all $Q\in\mathcal{N}^{**}_{\Gamma_{ij},\circ}$.

(ii) Case 2: $Q_i\in\mathcal{C}_i^{\Gamma_{ij}}$. The restriction of $\Phi_i\left(v^{Q_i}_{h,i}\right)$ to Γ_{ij} is a piecewise continuous polynomial of order 1 and is nonzero only on $e=QC_\sigma$ and $\widehat{e}=\widehat{Q}C_\sigma$ where Q and $\widehat{Q}$ belong to $\mathcal{N}^{**}_{\Gamma_{ij},\circ}$ for which (Q_i,Q,C_σ) and $(Q_i,\widehat{Q},C_\sigma)$ are elements of $\mathcal{T}^{**}_{h,i}$ (see Figure 5). Denote by $\mathcal{E}^{**,\mathcal{C}}_{\Gamma_{ij}}(Q_i)=\{QC_\sigma,\ \widehat{Q}C_\sigma\}$ then we use again the Simpson's rule to compute the integrals in (3.36) exactly:

$$\sum_{e\in\mathcal{E}^{**}_{\Gamma_{ij}}}\int_e\left(\Lambda_i\nabla_{\Lambda,i}u^{n+1}_{h,i}\cdot\boldsymbol{n}_{ij}+\alpha_{ij}\Phi_i(u^{n+1}_{h,i})\right)\Phi_i\left(v^{Q_i}_{h,i}\right)\,d\gamma$$

$$=\sum_{e\in\mathcal{E}^{**,\mathcal{C}}_{\Gamma_{ij}}(Q_i)}\frac{|e|}{6}\left\{\begin{array}{l}\left[2\Lambda_i\nabla_{\Lambda,i}u^{n+1}_{h,i}\cdot\boldsymbol{n}_{ij}|_e+\alpha_{ij}(u^{n+1}_{i,Q}+u^{Q,n}_{i,\sigma})\right]v^Q_{i,\sigma}\\ \left[\Lambda_i\nabla_{\Lambda,i}u^{n+1}_{h,i}\cdot\boldsymbol{n}_{ij}|_e+\alpha_{ij}u^{Q,n+1}_{i,\sigma}\right]v^Q_{i,\sigma}\end{array}\right\}$$

$$=\sum_{e\in\mathcal{E}^{**,\mathcal{C}}_{\Gamma_{ij}}(Q_i)}\frac{v^Q_{i,\sigma}}{6}\left\{\begin{array}{l}\displaystyle\int_e\left[\Lambda_i\nabla_{\Lambda,i}u^{n+1}_{h,i}\cdot\boldsymbol{n}_{ij}+\alpha_{ij}u^{n+1}_{i,Q}\right]d\gamma+\\ 2\displaystyle\int_e\left[\Lambda_i\nabla_{\Lambda,i}u^{n+1}_{h,i}\cdot\boldsymbol{n}_{ij}+\alpha_{ij}u^{Q,n+1}_{i,\sigma}\right]d\gamma\end{array}\right\}. \tag{3.54}$$

Similarly, we have

$$\sum_{e\in\mathcal{E}^{**}_{\Gamma_{ij}}}\int_e\left(\Lambda_j\nabla_{\Lambda,j}u^n_{h,j}\cdot\boldsymbol{n}_{ij}+\alpha_{ij}\Phi_j\left(u^n_{h,j}\right)\right)\Phi_j\left(E_{h,j}(v^{Q_i}_{i,\Gamma})\right)\,d\gamma$$

$$=\sum_{e\in\mathcal{E}^{**,\mathcal{C}}_{\Gamma_{ij}}(Q_i)}\frac{v^Q_{i,\sigma}}{6}\left\{\begin{array}{l}\displaystyle\int_e\left[\Lambda_j\nabla_{\Lambda,j}u^n_{h,j}\cdot\boldsymbol{n}_{ij}+\alpha_{ij}u^n_{j,Q}\right]d\gamma+\\ 2\displaystyle\int_e\left[\Lambda_j\nabla_{\Lambda,j}u^n_{h,j}\cdot\boldsymbol{n}_{ij}+\alpha_{ij}u^{Q,n}_{j,\sigma}\right]d\gamma\end{array}\right\}. \tag{3.55}$$

Combining (3.36), (3.37), (3.54) and (3.55), we deduce that (3.50) holds for $Q_i\in\mathcal{C}_i^{\Gamma_{ij}}$.

Now, we compute $B^{(2)}_{ij,n+1}$ exactly by using the Simpson's quadrature rule:

$$B^{(2)}_{ij,n+1} = \sum_{\substack{e\in\mathcal{E}^{**}_{\Gamma_{ij}}\\ e=QC_\sigma}} \int_e \left[\Lambda_i\nabla_{\Lambda,i}\varepsilon^{n+1}_{h,i}\cdot\boldsymbol{n}_{ij} + \alpha_{ij}\Phi_i(\varepsilon^{n+1}_{h,i})\right]^2 d\gamma$$

$$= \sum_{\substack{e\in\mathcal{E}^{**}_{\Gamma_{ij}}\\ e=QC_\sigma}} \frac{|e|}{6}\left\{\begin{array}{l} \left[\Lambda_i\nabla_{\Lambda,i}\varepsilon^{n+1}_{h,i}\cdot\boldsymbol{n}_{ij}|_e + \alpha_{ij}\varepsilon^{n+1}_{i,Q}\right]^2 + \\ \left[\Lambda_i\nabla_{\Lambda,i}\varepsilon^{n+1}_{h,i}\cdot\boldsymbol{n}_{ij}|_e + \alpha_{ij}\varepsilon^{n+1,Q}_{i,\sigma}\right]^2 + \\ 4\left[\Lambda_i\nabla_{\Lambda,i}\varepsilon^{n+1}_{h,i}\cdot\boldsymbol{n}_{ij}|_e + \alpha_{ij}\left(\dfrac{\varepsilon^{n+1}_{i,Q}+\varepsilon^{n+1,Q}_{i,\sigma}}{2}\right)\right]^2 \end{array}\right\}.$$

Using Equation (3.49) and the fact that $\boldsymbol{n}_{ij} = -\boldsymbol{n}_{ji}$, we deduce that

$$B^{(2)}_{ij,n+1} = \sum_{\substack{e\in\mathcal{E}^{**}_{\Gamma_{ij}}\\ e=QC_\sigma}} \frac{|e|}{6}\left\{\begin{array}{l} \left[\Lambda_j\nabla_{\Lambda,j}\varepsilon^{n}_{h,j}\cdot\boldsymbol{n}_{ji}|_e - \alpha_{ij}\varepsilon^{n}_{j,Q}\right]^2 + \left[\Lambda_j\nabla_{\Lambda,j}\varepsilon^{n}_{h,j}\cdot\boldsymbol{n}_{ji}|_e - \alpha_{ij}\varepsilon^{n,Q}_{j,\sigma}\right]^2 + \\ \left[\begin{array}{l} \left(\Lambda_j\nabla_{\Lambda,j}\varepsilon^{n}_{h,j}\cdot\boldsymbol{n}_{ji}|_e - \alpha_{ij}\varepsilon^{n}_{j,Q}\right)^2 + \left(\Lambda_j\nabla_{\Lambda,j}\varepsilon^{n}_{h,j}\cdot\boldsymbol{n}_{ji}|_e - \alpha_{ij}\varepsilon^{n,Q}_{j,\sigma}\right)^2 + \\ 2\left(\Lambda_j\nabla_{\Lambda,j}\varepsilon^{n}_{h,j}\cdot\boldsymbol{n}_{ji}|_e - \alpha_{ij}\varepsilon^{n}_{j,Q}\right)\left(\Lambda_j\nabla_{\Lambda,j}\varepsilon^{n}_{h,j}\cdot\boldsymbol{n}_{ji}|_e - \alpha_{ij}\varepsilon^{n,Q}_{j,\sigma}\right) \end{array}\right] \end{array}\right\}$$

$$= \int_{\Gamma_{ij}} \left[\Lambda_j\nabla_{\Lambda,j}\varepsilon^{n}_{h,j}\cdot\boldsymbol{n}_{ji} - \alpha_{ij}\Phi_j(\varepsilon^{n}_{h,j})\right]^2 d\gamma.$$

As $\alpha_{ij} = \alpha_{ji}$ (cf. Assumption (3.38)), we obtain:

$$B^{(2)}_{ij,n+1} = B^{(1)}_{ji,n}, \quad \text{for} \quad i,j = 1,...,N \text{ and } i \neq j.$$

Thus (3.48) becomes

$$A_{i,n+1} + \frac{1}{4\alpha_{ij}}B^{(1)}_{ij,n+1} = \frac{1}{4\alpha_{ji}}B^{(1)}_{ji,n}, \quad \text{for} \quad i,j = 1,...,N \text{ and } i \neq j. \tag{3.56}$$

We sum over all subdomains and over the iterates n, then let n go to infinity to obtain the following estimate:

$$\sum_{n=0}^{\infty}\sum_{i=1}^{N} A_{i,n+1} \leq \sum_{\substack{i,j=1\\ i\neq j}}^{N} \frac{1}{4\alpha_{ij}}B^{(1)}_{ij,0} \underset{(3.38)}{\leq} \frac{1}{4\alpha}\sum_{\substack{i,j=1\\ i\neq j}}^{N} B^{(1)}_{ij,0}, \tag{3.57}$$

where we have used the fact that $\displaystyle\sum_{\substack{i,j=1\\ i\neq j}}^{N} \frac{1}{4\alpha_{ij}}B^{(1)}_{ij,n} = \sum_{\substack{i,j=1\\ i\neq j}}^{N} \frac{1}{4\alpha_{ji}}B^{(1)}_{ji,n}$. The estimate (3.57) implies that the series $\displaystyle\sum_{n=0}^{\infty}\sum_{i=1}^{N} A_{i,n+1}$ is convergent and thus

$$\sum_{i=1}^{N} A_{i,n} = \sum_{i=1}^{N}\int_{\Omega_i} \left(\Lambda_i\nabla_{\Lambda,i}\varepsilon^{n}_{h,i}\right)\cdot\nabla_{\Lambda,i}\varepsilon^{n}_{h,i}d\boldsymbol{x} \to 0, \quad \text{when } n\to\infty. \qquad \square$$

4. Numerical experiments

We perform numerical experiments with discontinuous, isotropic or anisotropic coefficients to verify our theoretical results and investigate the performance of the optimized parameters for the case of two subdomains. The many subdomain case with cross points and coarse grid correction will be studied in our future work.

We consider a unit square $\Omega = [0,1]^2$ and its decomposition into two nonoverlapping subdomains: $\Omega_1 = [0, 1/2] \times [0,1]$ and $\Omega_2 = [1/2, 1] \times [0,1]$. The diffusion tensors are assumed to be constant in the subdomains and discontinuous across the interface. Two different mesh types are considered (see Figure 6): Type 1 is a structured mesh with rectangular primal elements and Type 2 an unstructured mesh with triangular primal elements. The associated dual sub-mesh for each type is shown in the same figure. In Table 1, the number of elements of the primal mesh $\mathcal{T}_h$ and the number of nodes of the dual sub-mesh $\mathcal{T}_h^{**}$ for different mesh size are presented. Recall that the FECC scheme has the same accuracy as the standard finite element method on the dual sub-mesh, however the computational cost is much lower since only primal cell unknowns are involved in the linear algebraic system [1]. Consequently, the scheme is cell-centered, and the errors presented in this section are computed in the L^2-norm on the primal mesh.

Mesh size h of $\mathcal{T}_h$		$h_1 = 1/8$	$h_2 = 1/16$	$h_3 = 1/32$	$h_4 = 1/64$	$h_5 = 1/128$
Type 1	#elements of $\mathcal{T}_h$	64	256	1024	4096	16384
	#nodes of $\mathcal{T}_h^{**}$	177	609	2241	8577	33537
Type 2	#elements of $\mathcal{T}_h$	224	896	3584	14336	57344
	#nodes of $\mathcal{T}_h^{**}$	385	1441	5569	21889	86785

Table 1: Numbers of elements of the primal mesh $\mathcal{T}_h$ and numbers of nodes of the dual sub-mesh $\mathcal{T}_h^{**}$ for different mesh sizes.

We first study the error equation with isotropic diffusion tensors in Subsection 4.1. Convergence of the iterative algorithms with optimized Robin parameters is investigated with respect to different jumps in the coefficients, different mesh sizes and different iterative solvers. In Subsection 4.2, we consider a problem with a known analytical solution and with anisotropic, discontinuous diffusion tensor, and verify the convergence and order of accuracy of the domain decomposition-based FECC scheme.

4.1. Test case 1: with isotropic, discontinuous diffusion tensors

The diffusion matrix is defined as $\Lambda(\boldsymbol{x}) = \Lambda_i$ for $\boldsymbol{x} \in \Omega_i$, $i = 1, 2$, where $\Lambda_i = \lambda_i \boldsymbol{I}$, and $\boldsymbol{I}$ is the 2D identity tensor. We fix $\lambda_1 = 1$ and vary $\lambda_2 \in \{10, 100, 1000\}$. Denote by $r := \lambda_2/\lambda_1$ the diffusion ratio. We solve the error equation with a zero solution:

$$\begin{aligned} -\text{div } (\Lambda(\boldsymbol{x})\nabla\varepsilon(\boldsymbol{x})) &= 0 \quad \text{in } \Omega, \\ \varepsilon &= 0 \quad \text{on } \partial\Omega. \end{aligned}$$

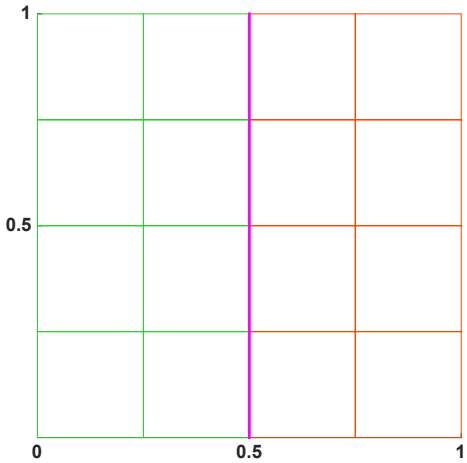

Primal mesh $\mathcal{T}_h$, type 1.

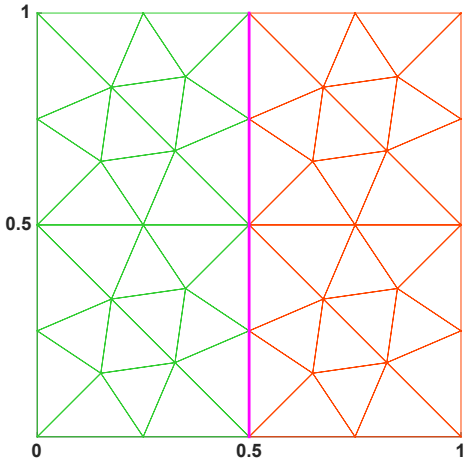

Primal mesh $\mathcal{T}_h$, type 2.

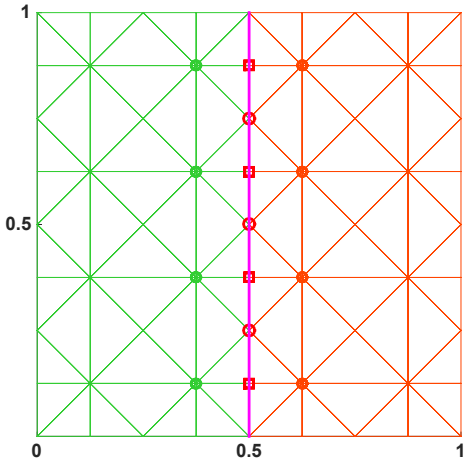

Dual sub-mesh $\mathcal{T}_h^{**}$, type 1.

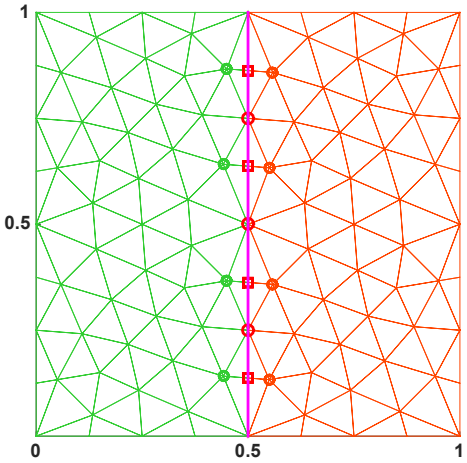

Dual sub-mesh $\mathcal{T}_h^{**}$, type 2.

Figure 6: The primal meshes and its dual sub-meshes for Type 1 (left) and Type 2 (right) respectively.

The problem is reformulated as an interface problem as in Section 3, Equation (3.33), which is solved iteratively by either Jacobi or GMRES. We start with a random initial guess and at each iteration, we calculate the normalized error in $L^2(\Omega)-$ norm, $(\|\boldsymbol{\varepsilon}_h^n\|_2/\|\boldsymbol{\varepsilon}_h^0\|_2)$.

As the problem involves discontinuous coefficients, one should use different optimized parameters $\alpha_{12} \neq \alpha_{21}$, namely *two-sided* Robin parameters, to take into account the different physical parameters. Recall that in Subsection 3.3, in order to prove the convergence of the Robin-to-Robin algorithm (corresponding to solving the interface problem by Jacobi method), we have assumed that these parameters are equal (cf. Assumption (3.38)), i.e. *one-sided* Robin parameters: $\alpha_{12} = \alpha_{21} = \alpha$. However, in practice, this assumption is usually not required. We refer to [42, Chapter 3] for a detailed calculation of one-sided and two-sided optimized Robin parameters.

To study the performance of different types of optimized parameters with FECC discretization, we fix $h = h_2$ and consider the mesh of type 1. In Figure 8, we plot the L^2-error, computed by using one-sided and two-sided optimized Robin parameters, versus the number of iterations using Jacobi (on the left) and GMRES (on the right), for different diffusion ratios, $r \in \{10, 100, 1000\}$. We observe that all algorithms work well. Concerning the one-sided Robin case, the convergence deteriorates as the diffusion ratio increases, especially when solving by Jacobi method; in addition, we see that GMRES speeds up significantly the convergence - the number of GMRES iterations is much smaller than that of Jacobi iterations, especially for large diffusion ratios. On the contrary, when the two-sided optimized Robin parameters are used, the larger the diffusion ratio the faster the convergence, and GMRES also improves the convergence speed compared to Jacobi iteration but not as profoundly as in the case of one-sided Robin parameters. The results confirm that the use of two-sided optimized Robin parameters is more efficient than one-sided Robin parameters, especially for large discontinuities in the coefficients. Note that these results are obtained with optimized parameters which are calculated by numerically minimizing the continuous convergence factor [26, 42]. To verify the performance of the optimized Robin parameters in the framework of the FECC scheme, we vary α for the one-sided Robin, or vary α_{12} and α_{21} for the two-sided Robin, and compute the number of Jacobi iterations required to achieve a relative residual 10^{-6}. The results are shown in Figure 8 where we see that both one-sided and two-sided optimized Robin parameters (the red stars) are located close to those giving the smallest number of iterations for the same tolerance.

Next, we study the convergence of the iterative algorithms with respect to different mesh sizes. In the following, we shall only use two-sided optimized Robin parameters to efficiently deal with discontinuous coefficients. Tables 2 and 3 show the numbers of Jacobi and GMRES iterations required to reach an error reduction 10^{-6} for mesh type 1 and type 2 respectively. The results are for different diffusion ratios and different mesh sizes. We observe again that the larger the diffusion ratio the faster the convergence, and for large diffusion ratios, the convergence is almost independent of the mesh size. This is obtained because of the optimized parameters which play a role as a preconditioner when solving iteratively the interface problem. Note that the results agree with the theoretical

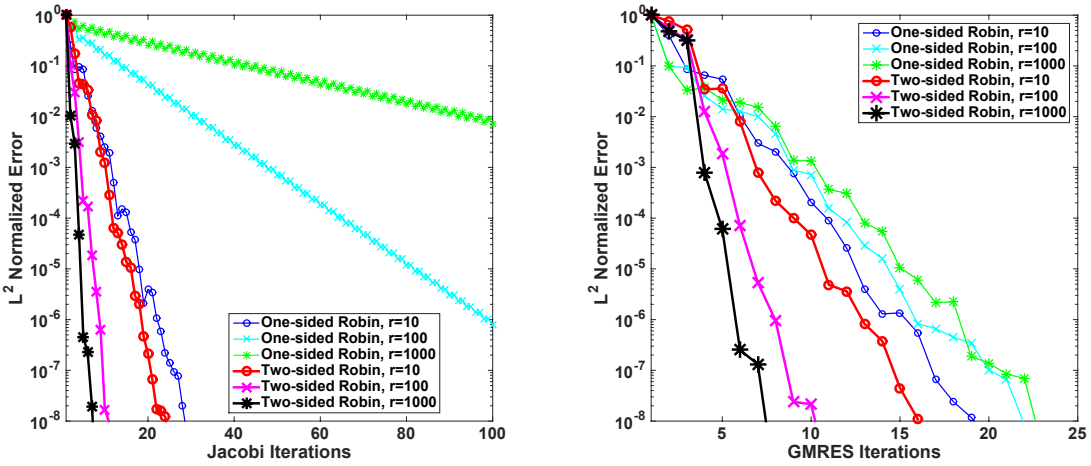

Figure 7: Convergence curves obtained by one-sided and two-sided optimized parameters for different diffusion ratios: Jacobi iterations (left) and GMRES iterations (right).

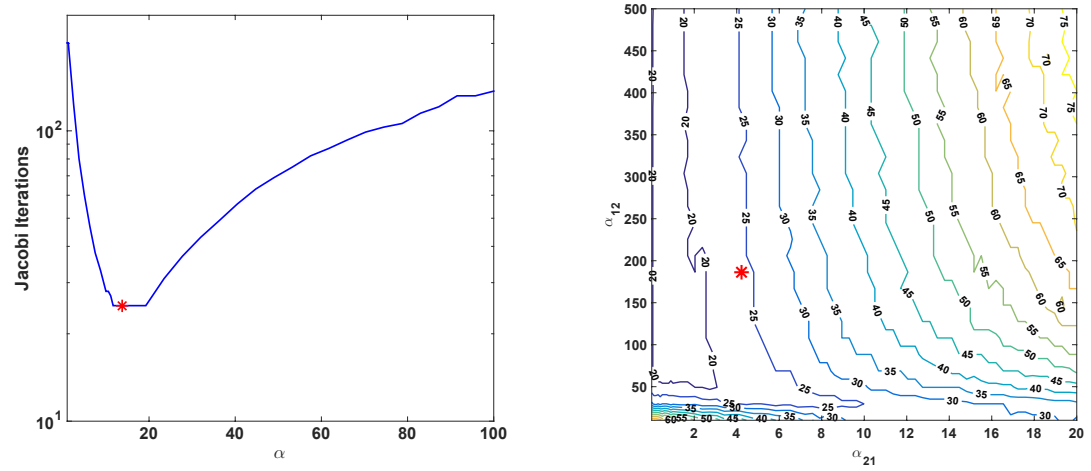

Figure 8: Level curves for the number of Jacobi iterations required to reach a relative residual of 10^{-6} for various values of one-sided (left) and two-sided (right) Robin parameters. The red star shows the optimized parameters.

asymptotic performance of the optimized Robin transmission conditions proved in [26]. In particular, the convergence factor of Jacobi iterations behaves like $1 - O(h^{1/2})$ and $1 - O(h^{1/4})$ for the one-sided and two-sided parameters, respectively, while for GMRES solver, the asymptotic performance is improved by a square root. Additionally, we see that if the number of Jacobi iterations is large, then GMRES would improve significantly the convergence; however, if Jacobi converges fast, then GMRES would converge at the same speed. The results for mesh type 1 and mesh type 2 are quite similar.

Diffusion	h_1		h_2		h_3		h_4	
ratio r	Jacobi	GMRES	Jacobi	GMRES	Jacobi	GMRES	Jacobi	GMRES
10	15	12	19	13	25	15	35	18
100	8	7	9	8	10	9	11	10
1000	5	6	5	6	7	6	7	8

Table 2: Number of Jacobi iterations and GMRES iterations required to reach an error reduction 10^{-6} for mesh type 1 (Test case 1). The results are obtained using two-sided optimized Robin parameters.

Diffusion	h_1		h_2		h_3		h_4	
ratio r	Jacobi	GMRES	Jacobi	GMRES	Jacobi	GMRES	Jacobi	GMRES
10	16	12	21	14	27	16	41	20
100	8	8	9	9	11	10	13	11
1000	6	6	6	6	7	7	8	8

Table 3: Number of Jacobi iterations and GMRES iterations required to reach an error reduction 10^{-6} for mesh type 2 (Test case 1). The results are obtained using two-sided optimized Robin parameters.

4.2. Test case 2: with an anisotropic, discontinuous diffusion tensor

We consider the diffusion problem with an exact solution given by

$$u_{\text{exact}} = \begin{cases} \cos(\pi x)\sin(\pi y) & \text{if } x \le 0.5, \\ 10^{-2}\cos(\pi x)\sin(\pi y) & \text{if } x > 0.5, \end{cases}, \quad \text{with } \Lambda = \begin{cases} \boldsymbol{I} & \text{if } x \le 0.5, \\ \begin{bmatrix} 10^2 & 0 \\ 0 & 0.01 \end{bmatrix} & \text{if } x > 0.5. \end{cases}$$

For this case, we solve the interface problem iteratively with a zero initial guess, and stop the iteration when the relative residual is smaller than 10^{-6}. Then we compute the relative errors between the "converged" multidomain solution and the exact solution in L^2-norm on the primal mesh. Again, two-sided optimized Robin parameters are considered. We observe that even for anisotropic, discontinuous coefficients, the proposed domain decomposition-based FECC method with optimized Robin transmission conditions is very efficient and requires only a few number of Jacobi/GMRES iterations for convergence no matter how small the mesh size is. The "converged" multidomain solution is second-order accurate as

expected. Figure 9 shows that the optimized Robin parameters perform very well either with zero or random initial guesses (with a fixed mesh size $h = h_2$). In addition, we compute numerically the total fluxes across the interface edges of the "converged" multidomain solution and obtain 8.515E-7, which is smaller than the tolerance. This confirms that the local flux continuity property of the FECC method is preserved with Robin transmission conditions derived in Section 3.2.

h	Mesh type 1			Mesh type 2		
	Jacobi iterations	GMRES iterations	L^2 error [CR]	Jacobi iterations	GMRES iterations	L^2 error [CR]
h_1	9	5	4.490E-2	9	6	5.007E-3
h_2	11	5	1.163E-2 [1.95]	11	7	1.291E-3 [1.96]
h_3	11	6	3.007E-3 [1.95]	11	7	3.324E-4 [1.96]
h_4	13	7	7.691E-4 [1.97]	13	7	8.477E-5 [1.97]
h_5	15	7	1.948E-4 [1.98]	13	7	2.148E-5 [1.98]

Table 4: Number of Jacobi and GMRES iterations required to reach a relative residual of 10^{-6}, corresponding L^2 errors and convergence rates (Test case 2).

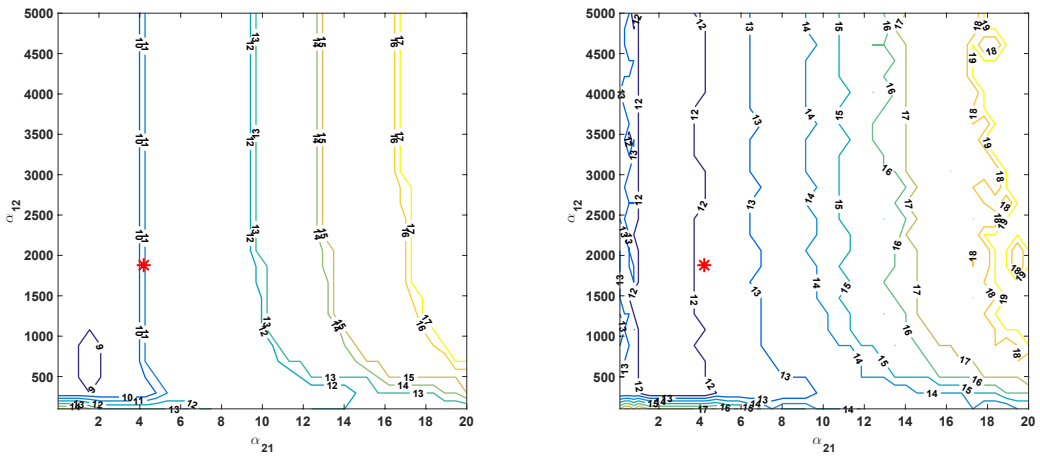

Figure 9: Level curves for the number of Jacobi iterations required to reach a relative residual of 10^{-6} for various values of two-sided Robin parameters with zero (left) and random (right) initial guesses. The red star shows the optimized parameters.

5. Conclusions

We have formulated a nonoverlapping domain decomposition method with Robin-type transmission conditions for heterogeneous, anisotropic diffusion problems discretized by the

FECC method. The new transmission conditions consist of both weak and strong forms of the Robin terms because of the construction of the discrete gradient operator involved in the FECC method. A discrete interface problem associated with such transmission conditions is derived. Solving the interface problem iteratively by Jacobi method results in the so-called Robin-to-Robin iterative algorithm which is proved to be convergent for the case of multiple strip-shaped subdomains. Numerical results for 2D problems in which optimized Robin parameters are used and the interface problem is solved by either Jacobi or GMRES methods are presented. We have analyzed numerically the performance of the proposed method for both isotropic and anisotropic diffusion tensors with large discontinuities in the coefficients. We have observed that the two-sided optimized Robin parameters handle well the heterogeneity and anisotropy, and only a few number of iterations is required to achieve desired accuracy. Even though the optimized parameters are derived based on the continuous convergence factor, they still work well for the mixed Robin transmission conditions in the framework of FECC scheme. They play the role as a preconditioner for the interface problem, which helps the convergence of the iterations almost independent of the mesh size, especially for large jumps in the coefficients. Work underway addresses the multiple subdomain case with cross points as well as three dimensional diffusion problems with general meshes.

References

[1] C. Le Potier, T. H. Ong, A cell-centered scheme for heterogeneous anisotropic diffusion problems on general meshes, International Journal on Finite Volumes 8 (2012) pp. 1–40.

[2] T. H. Ong, Cell-centered scheme for heterogeneous anisotropic diffusion problems on general meshes, PhD thesis, Université Paris-Est, 2012.

[3] I. Aavatsmark, T. Barkve, O. Bøe, T. Mannseth, Discretization on unstructured grids for inhomogeneous, anisotropic media. Part I: Derivation of the methods, SIAM Journal on Scientific Computing 19 (5) (1998) pp. 1700–1716.

[4] Z. Cai, On the finite volume element method, Numer. Math 58 (1991) 713–735.

[5] Z. Cai, L. Mandel, S. McCormick, The finite volume element method for diffusion equations on general triangulations, SIAM J. Num. Anal. 28 (2) (1991) 392–402.

[6] R. Li, Z. Chen, W. Wu, Generalized difference methods for differential equations: numerical analysis of finite volume methods, CRC Press, 2000.

[7] G. Anasanay-Alex, B. Piar, D. Vola, A Galerkin finite element solution, in: R. Eymard, J. Hérard (Eds.), Finite Volumes for Complex Applications V, John Wiley & Sons, 2008, pp. 717–733.

[8] L. Agelas, D. Di Pietro, A symmetric finite volume scheme for anisotropic heterogeneous second-order elliptic problems, in: R. Eymard, J. Hérard (Eds.), Benchmark on Anisotropic Problems, Finite Volumes for Complex Applications V, John Wiley & Sons, 2008, pp. 705–716.

[9] C. Le Potier, Numerical results with two cell-centered finite volume schemes for heterogeneous anisotropic diffusion operators, in: R. Eymard, J. Hérard (Eds.), Finite Volumes for Complex Applications V, John Wiley & Sons, 2008, pp. 825–842.

[10] C. Chainais-Hillairet, J. Droniou, R. Eymard, Use of mixed finite volume method, in: R. Eymard, J. Hérard (Eds.), Finite Volumes for Complex Applications V, John Wiley & Sons, 2008, pp. 751–760.

[11] K. Lipnikov, Mimetic finite difference method, in: R. Eymard, J. Hérard (Eds.), Finite Volumes for Complex Applications V, John Wiley & Sons, 2008, pp. 801–814.

[12] S. Mundal, D. Di Pietro, I. Aavatsmark, Compact-stencil MPFA method for heterogeneous highly anisotropic second-order elliptic problems, in: R. Eymard, J. Hérard (Eds.), Finite Volumes for Complex Applications V, John Wiley & Sons, 2008, pp. 905–918.

[13] F. Hermeline, Numerical experiments with the DDFV method, in: R. Eymard, J. Hérard (Eds.), Finite Volumes for Complex Applications V, John Wiley & Sons, 2008, pp. 851–864.

[14] R. Eymard, T. Gallouët, R. Herbin, Discretization of heterogeneous and anisotropic diffusion problems on general non-conforming meshes. Sushi: A Scheme Using Stabilization and Hybrid Interfaces, IMA Journal of Numerical Analysis 30 (4) (2010) 1009–1034.

[15] T. H. Ong, T.-T.-P. Hoang, S. Bordas, H. Nguyen-Xuan, A staggered cell-centered finite element method for compressible and nearly-incompressible linear elasticity on general meshes, SIAM J. Numer. Anal. 53 (4) (2015) 2051–2073.

[16] T.-T.-P. Hoang, D. C. H. Vo, T. H. Ong, A low-order finite element method for three dimensional linear elasticity problems with general meshes 74 (6) (2017) 1379–1398.

[17] A. Quarteroni, A. Valli, Domain decomposition methods for partial differential equations, Clarendon Press, Oxford New York, 1999.

[18] A. Toselli, O. Widlund, Domain decomposition methods—algorithms and theory, Vol. 34 of Springer Series in Computational Mathematics, Springer-Verlag, 2005.

[19] T. Mathew, Domain decomposition methods for the numerical solution of partial differential equations, Vol. 61 of Lecture Notes in Computational Science and Engineering, Springer, 2008.

[20] V. Agoshkov, Poincaré-Steklov's operators and domain decomposition methods in finite-dimensional spaces, First International Symposium on Domain Decomposition Methods for Partial Differential Equations (Paris), SIAM, Philadelphia, PA, 1988, pp. 73–112.

[21] A. Quarteroni, A. Valli, Theory and application of Steklov-Poincaré operators for boundary-value problems: the heterogeneous operator case, Fourth International Symposium on Domain Decomposition Methods for Partial Differential Equations (Moscow), SIAM, 1991, pp. 58–81.

[22] R. Glowinski, M. Wheeler, Domain decomposition and mixed finite element methods for elliptic problems, First International Symposium on Domain Decomposition Methods for Partial Differential Equations (Paris), SIAM, 1988, pp. 144–172.

[23] P. Lions, On the Schwarz alternating method. III: A variant for nonoverlapping subdomains., Third International Symposium on Domain Decomposition Methods for Partial Differential Equations (Houston), SIAM, 1990, pp. 202–223.

[24] F. Nataf, F. Rogier, Factorization of the convection-diffusion operator and the Schwarz algorithm, Math. Models Methods Appl. Sci. 5 (1) (1995) 67–93.

[25] C. Japhet, F. Nataf, F. Rogier, The Optimized Order 2 method. application to convection-diffusion problems, Future Gener. Comp. Sy. 18 (1) (2001) 17–30.

[26] M. Gander, Optimized Schwarz methods, SIAM J. Numer. Anal. 44 (2) (2006) 699–731.

[27] D. Bennequin, M. J. Gander, L. Halpern, A homographic best approximation problem with application to optimized Schwarz waveform relaxation, Math. Comp. 78 (265) (2009) 185–223.

[28] F. Boyer, F. Hubert, S. Krell, Non-overlapping Schwarz algorithm for solving 2d m-DDFV schemes, IMA Journal of Numerical Analysis 30 (4) (2010) 1062–1100.

[29] L. Gerardo-Giorda, F. Nataf., Optimized Schwarz methods for unsymmetric layered problems with strongly discontinuous and anisotropic coefficients, J. Numer. Math. 13 (4) (2005) 265 – 294.

[30] E. Flauraud, F. Nataf, F. Willien, Optimized interface conditions in domain decomposition methods for problems with extreme contrasts in the coefficients, Journal of Computational and Applied Mathematics 189 (1) (2006) 539 – 554, proceedings of The 11th International Congress on Computational and Applied Mathematics.

[31] Y. Maday, F. Magoules, Optimized Schwarz methods without overlap for highly heterogeneous media, Comput. Methods Appl. Mech. Eng. 196 (8) (2007) 1541 – 1553.

[32] M. J. Gander, O. Dubois, Optimized Schwarz methods for a diffusion problem with discontinuous coefficient, Numer. Algor. 69 (1) (2015) 109–144.

[33] M. J. Gander, L. Halpern, M. Kern, A Schwarz waveform relaxation method for advection-diffusion-reaction problems with discontinuous coefficients and non-matching grids, in: Domain decomposition methods in science and engineering XVI, Vol. 55 of Lect. Notes Comput. Sci. Eng., Springer, Berlin, 2007, pp. 283–290.

[34] E. Blayo, L. Halpern, C. Japhet, Optimized Schwarz waveform relaxation algorithms with nonconforming time discretization for coupling convection-diffusion problems with discontinuous coefficients, in: Domain decomposition methods in science and engineering XVI, Vol. 55 of Lect. Notes Comput. Sci. Eng., Springer, Berlin, 2007, pp. 267–274.

[35] L. Halpern, C. Japhet, J. Szeftel, Optimized Schwarz waveform relaxation and discontinuous Galerkin time stepping for heterogeneous problems, SIAM J. Numer. Anal. 50 (5) (2012) 2588–2611.

[36] C. Japhet, P. Omnes, Optimized Schwarz waveform relaxation for porous media applications, in: T. J. Barth, M. Griebel, D. E. Keyes, R. M. Nieminen, D. Roose, T. Schlick (Eds.), Decomposition Methods in Science and Engineering XX, Vol. 91 of Lecture Notes in Computational Science and Engineering, Springer, 2013, pp. 585–592.

[37] T.-T.-P. Hoang, J. Jaffré, C. Japhet, M. Kern, J. E. Roberts, Space-time domain decomposition methods for diffusion problems in mixed formulations, SIAM J. Numer. Anal. 51 (6) (2013) 3532–3559.

[38] E. Blayo, L. Debreu, F. Lemarié, Toward an optimized global-in-time Schwarz algorithm for diffusion equations with discontinuous and spatially variable coefficients. Part 2: the variable coefficients case, ETNA 40 (2013) 170–186.

[39] M. J. Gander, K. Santugini-Repiquet, Cross-points in domain decomposition methods with a finite element discretization, Electron. T. Numer. Ana. 45 (2016) 219–240.

[40] M. J. Gander, F. Kwok, On the applicability of Lions energy estimates in the analysis of discrete optimized Schwarz methods with cross points, in: B. R., H. M., W. O., X. J. (Eds.), Domain decomposition methods in science and engineering XX, Vol. 91 of Lect. Notes Comput. Sci. Eng., Springer, Berlin, 2013, pp. 475–483.

[41] P. Ciarlet, The finite element method for elliptic problems, North-Holland Pub. Co. Sole distributors for the U.S.A. and Canada, Elsevier North-Holland, Amsterdam New York, 1980.

[42] O. Dubois, Optimized Schwarz methods for the advection-diffusion equation and for problems with discontinuous coefficients, PhD thesis, McGill University, 2007.